



HAL
open science

Near-infrared emissive bacteriochlorin-diketopyrrolopyrrole triads: Synthesis and photophysical properties

Flavien Ponsot, Nicolas Desbois, Léo Bucher, Mathieu Berthelot, Pritam Mondal, Claude P Gros, Anthony Romieu

► **To cite this version:**

Flavien Ponsot, Nicolas Desbois, Léo Bucher, Mathieu Berthelot, Pritam Mondal, et al.. Near-infrared emissive bacteriochlorin-diketopyrrolopyrrole triads: Synthesis and photophysical properties. *Dyes and Pigments*, 2019, 160, pp.747-756. 10.1016/j.dyepig.2018.08.059 . hal-03476108

HAL Id: hal-03476108

<https://hal.science/hal-03476108>

Submitted on 12 Dec 2021

HAL is a multi-disciplinary open access archive for the deposit and dissemination of scientific research documents, whether they are published or not. The documents may come from teaching and research institutions in France or abroad, or from public or private research centers.

L'archive ouverte pluridisciplinaire **HAL**, est destinée au dépôt et à la diffusion de documents scientifiques de niveau recherche, publiés ou non, émanant des établissements d'enseignement et de recherche français ou étrangers, des laboratoires publics ou privés.

Near-infrared emissive bacteriochlorin-diketopyrrolopyrrole triads: Synthesis and photophysical properties

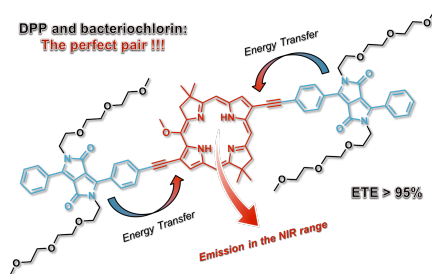
Flavien Ponsot^a, Nicolas Desbois^a, Léo Bucher^a, Mathieu Berthelot^a, Pritam Mondal^a, Claude P. Gros^{a,*}, Anthony Romieu^{a,b,*}

^aInstitut de Chimie Moléculaire de l'Université de Bourgogne, UMR 6302, CNRS, Univ. Bourgogne Franche-Comté, 9, Avenue Alain Savary, 21078 Dijon cedex, France

^bInstitut Universitaire de France, 1, Rue Descartes, Bâtiment MONGE, 75005 Paris, France

Abstract The synthesis of unprecedented energy transfer triads containing a near-infrared (NIR) emissive bacteriochlorin subunit and two diketopyrrolopyrrole (DPP) moieties linked to each other *via* ethynyl or zero-carbon spacers is presented. Their optical and fluorescence properties were determined in CHCl₃ and toluene. These photophysical measurements highlight the ability of DPP scaffold to act as an effective energy donor, which once excited in the range 450-550 nm resulting nearly exclusively NIR emission of hydrophorphyrin (ETE > 96%). Since DPP dyes are valuable structurally tunable fluorophores that may be used in the construction of high-performance multicomponent photoactive systems, their spectral compatibility with bacteriochlorin chromophore demonstrated through this work, is an important first step toward the rational design of novel and innovative hybrid NIR fluorophores inspired by (bacterio)chlorophylls and suitable for biomedical applications.

Graphical abstract



Keywords Bacteriochlorin, Diketopyrrolopyrrole, Energy-transfer triad, Fluorophore, Near-infrared fluorescence

Highlights

Synthesis of first bacteriochlorin-DPP triads *via* Pd-catalyzed cross-coupling reactions

Investigation of photophysical properties in organic solvents

Nearly quantitative S₁-S₁ energy transfer between DPP and bacteriochlorin in triads

* Corresponding authors.

E-mail address: claude.gros@u-bourgogne.fr or anthony.romieu@u-bourgogne.fr

1. Introduction

One of the growing trends in medicine is increased emphasis on early detection of disease in order to administer timely treatment that will improve the prognosis of the patient. Of the emerging diagnostic techniques, biomedical imaging has proven to be superior to traditional diagnostic methods due to its minimal invasiveness, absence of side effects, rapid results, and identification of possible mechanisms of pathological presentation through elucidation of internal biomolecular structure and shape[1,2]. Therefore, great efforts have been made to improve contrast agents and imaging techniques. Quite special interest was paid to fluorescence modality because of its numerous advantages (*i.e.*, convenience, sensitivity, cost-effectiveness, safety, and non-radioactive material safety), especially for molecular imaging in preclinical studies. Indeed, illumination of receptors, enzymes, gene expression, *in vitro* live cells, and tumors cells *in vivo* is a valuable approach to gain a sound understanding of disease progression and therapeutic response at the molecular, cell, tissue, and whole-animal levels[3,4]. However, all or part of these valuable features are jeopardized when *in vivo* fluorescence imaging uses traditional wavelengths in the visible spectrum. Indeed, substantial photon scattering and/or photon absorption by biological tissues, coupled with significant interferences from tissue auto-fluorescence occur and contribute to the dramatic loss of signal and the gain of background noise. The use of near-infrared (NIR) fluorescent probes, having absorption/emission maxima in the spectral range 700-900 nm, often called "therapeutic optical window" (or NIR-I window), optimal brightness and photostability, has proven to be an effective way to overcome these limitations and to achieve deep-tissue analyses[5-7]. During the past two decades, intensive research efforts have been devoted to the development of a wide range of long wavelength photoactive (bio)molecular structures satisfying all or part of these specifications[8-10]. Among the different classes of NIR fluorescent labels currently available, organic-based fluorophores have a prominent place and are often preferred for bioimaging applications based on the use of activatable (or "smart") fluorescent probes[11-13]. Indeed, the design of NIR analyte-responsive chemodosimeters on the basis of well-known photophysical processes and/or fluorogenic reactions is much easier (or only possible) with organic fluorophore platforms than with fluorescent proteins, semi-conductor nanocrystals (quantum dots) or nanomaterials (*e.g.*, inorganic upconverting nanoparticles). The families of NIR fluorophores emitting above 700 nm have been so far dominated by the cyanine (*i.e.*, Cy7 derivatives)[14,15]

and (aza-)BODIPY dyes[16], even if silicon-substituted xanthenes and dihydroxanthene-hemicyanine hybrids have recently emerged as valuable alternatives to these "golden imaging standards"[17-19]. Furthermore, design strategies inspired by biomolecules or natural products responsible of the far-red or NIR fluorescence observed in some biological systems, have recently emerged[15],[20-22]. The major contribution of the Lindsey group focused on the development of biocompatible fluorophores with a chemical structure that is related to the photosynthetic pigments (*i.e.*, chlorins[23] and bacteriochlorins (BC)[24]) deserves to be highlighted[25-34]. However, the synthetic access to these hydroporphyrin derivatives and their site-specific functionalization(s) are often a true priesthood[35-38]. Thus, in order to simplify the preparation of high-performance engineered NIR fluorophores based on a (bacterio)chlorin scaffold without resorting to tedious *de novo* syntheses, we plan to explore a chromophore merging-based strategy leading to unprecedented hybrids structures between hydroporphyrin and diketopyrrolopyrrole (DPP) photoactive units (Fig. 1)[39-48]. Indeed, in view of their outstanding properties (high fluorescence quantum yields, large two-photon absorption cross-sections and exceptional chemical, light and thermal stability) and their facile synthesis and functionalization, DPP dyes have recently emerged as valuable alternatives to conventional visible fluorophores[49,50]. Their integration with porphyrin-like molecules should facilitate the introduction of specific functionalities usually required for biosensing/bioimaging (*i.e.*, a bioconjugatable tether, water-solubilizing groups and possibly an optically tunable reactive group for modulation of fluorescence properties), and through a highly modular approach. Furthermore, depending on the linker chosen for the attachment of 3,6-diaryl-substituted DPP units to 13- (or 3,13-) positions of hydrophorphyrin (*i.e.*, alkynyl, dimethine or zero-carbon bridge), we intend to obtain either energy transfer (ET) dyads/triads characterized by a negligible electronic conjugation between chromophores, or strongly π -conjugated BC-DPP hybrids with extended NIR absorption/emission compared to those of more conventional synthetic BCs (Fig. 1). To the best of our knowledge, this proposed novel class of NIR organic-based fluorophores has never been reported in the literature although in recent years, there is a growing interest for the synthesis and overall photophysical and redox characterization of energy transfer dyads bearing a synthetic BC unit as the energy acceptor, with the aim of providing efficient panchromatic molecular assemblies for light-harvesting and solar cells applications[51-56]. The vast majority of these ET dyads involve a chlorin, a BODIPY or a perylene-monoimide unit as the energy donor. Interestingly, this ET strategy is also particularly

suited to artificially and dramatically increase the Stokes' shift (pseudo-Stokes' shift in the range 85-110 nm) of BCs which is typically less than 10 nm, regardless of the solvent, substitution pattern and metalation state of these macrocycles. This is a valuable and essential feature to minimize self-quenching and fluorescence detection errors stemming from excitation backscattering effects, and for possible applications of hydroporphyrins in NIR fluorescence molecular imaging[20-22,27].

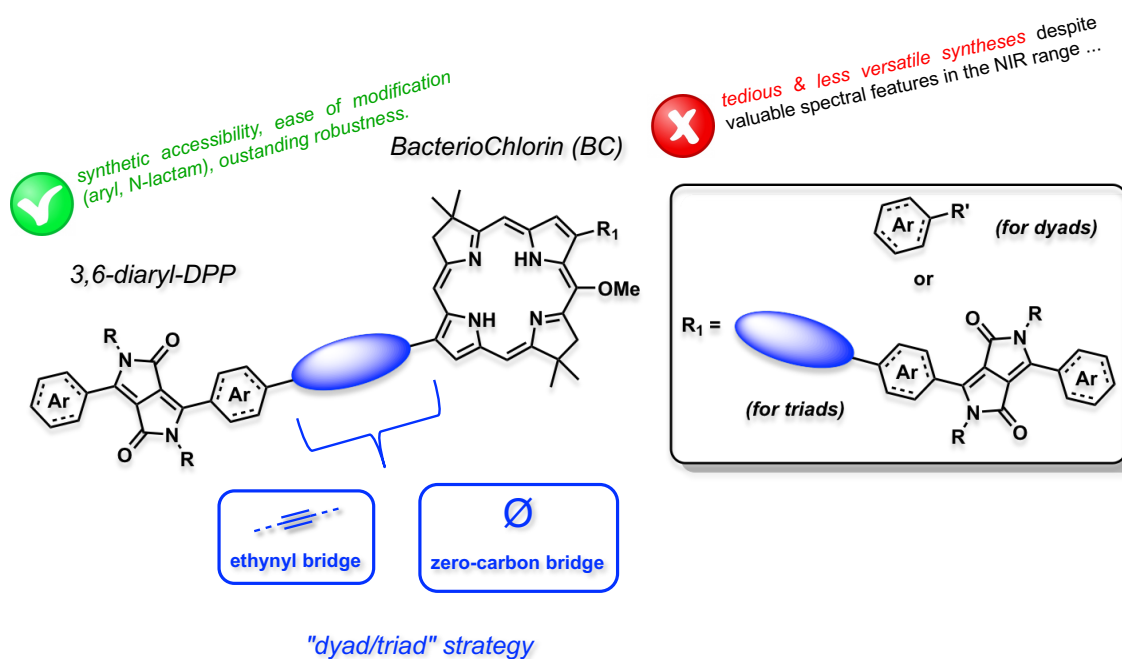


Fig. 1. Schematic overview of the molecular design strategy toward BC-DPP hybrid NIR fluorophores. *Please note: the term "zero-carbon bridge" means that the covalent connection between bacteriochlorin and DPP units involves the sole aryl substituent of this latter chromophore. The present work only discloses the synthesis of triads involving two donor DPP units and not dyads.*

It is in this context that we report herein the first synthesis and basic photophysical studies of three BC-DPP energy transfer triads differentiated by the linker connecting the chromophoric units (*i.e.*, ethynyl or zero-carbon bridge) and/or DPP substitution pattern (*i.e.*, 3,6-diaryl and *N*-lactam substituents).

2. Experimental

2.1 Chemicals and instruments

Unless otherwise noted, all commercially available reagents and solvents were used without

further purification. TLC were carried out on Merck DC Kieselgel 60 F-254 aluminum sheets. The spots were directly visualized or through illumination with UV lamp ($\lambda = 254/365$ nm). Column chromatography purifications were performed on silica gel (40-63 μm and 63-200 μm) from Sigma-Aldrich (technical grade). Size-exclusion chromatography purifications were performed with Bio-Beads[®] S-X3 support (ca. 125 g for up to 200 mg of dye, 40 \times 450 mm bed) from Bio-Rad (#152-2750). THF (HPLC-grade, Biosolve) was dried over alumina cartridges using a solvent purification system PureSolv PS-MD-5 model from Innovative Technology. Dry TEA was obtained by distillation over CaH_2 and stored under argon on 3 \AA molecular sieves. The following compounds were prepared according to literature procedure: 3,13-dibromo-5-methoxy-8,8,18,18-tetramethyl-bacteriochlorin (**diBr-BC**, [CAS: 1006370-88-2])[57], TMS-ethynyl thienyl-DPP dye **1** (CAS: 1637582-58-1)[58], unsymmetrical phenyl-DPP pigment **2** [CAS: 112026-72-9][59] and 3,6-diphenyl-DPP pigment [CAS: 54660-00-3][60].

^1H - and ^{13}C -NMR spectra were recorded on a Bruker Avance 500 spectrometer. Chemical shifts are expressed in parts per million (ppm) from the residual non-deuterated CHCl_3 signal[61]. J values are expressed in Hz. IR spectra were recorded with a Bruker Alpha FT-IR spectrometer equipped with a universal ATR sampling accessory. The bond vibration frequencies are expressed in reciprocal centimeters (cm^{-1}). Low- and high-resolution mass spectra (LRMS and HRMS) were recorded either with a Bruker Daltonics Ultraflex II LRF 2000 mass spectrometer (MALDI-TOF, matrix: dithranol) or a Bruker Amazon SL instrument equipped with an electrospray (ESI) source or a Thermo Scientific MSQ Plus single quadrupole equipped with an ESI source (parameters for the ESI-MS analysis of BC-DPP triads: probe temperature: 350 $^\circ\text{C}$, needle: 3.0 kV, detector: 1153 V and cone voltage: 200 V). UV-visible spectra were obtained either on a Varian Cary 50 scan (single-beam) or an Agilent Cary 5000 UV-VIS-NIR (double beam) spectrophotometer by using a rectangular quartz cell (Hellma, 100-QS, 45 \times 12.5 \times 12.5 mm, pathlength: 10 mm, chamber volume: 3.5 mL), at 25 $^\circ\text{C}$ (using a temperature control system combined with water circulation). Fluorescence spectroscopic studies (Em./Ex. spectra and kinetics) were performed with an HORIBA Jobin Yvon Fluorolog spectrofluorometer (software FluorEssence) at 25 $^\circ\text{C}$ (using a temperature control system combined with water circulation), with a standard fluorometer cell (Labbox, LB Q, light path: 10 mm, width: 10 mm, chamber volume: 3.5 mL). See ESI for all experimental details related to photophysical characterizations of DPP dyes and BC-DPP triads.

2.2 Synthesis of functionalized BC and DPP derivatives

2.2.1 Ethynyl-functionalized thienyl-DPP [CAS: 1637582-59-2] (**1**)

To a solution of TMS-ethynyl thienyl-DPP[58] (37.0 mg, 59.6 μmol , 1.0 equiv) in THF (8 mL) and deionized water (4 mL), solid KF (17.3 mg, 298 μmol , 5.0 equiv) was added. The resulting mixture was stirred at RT and under argon for 3 h. Then, aq. saturated NH_4Cl (50 mL) was added and the desired product was extracted thrice with CH_2Cl_2 . The combined organic layers were washed with brine, dried over anhydrous Na_2SO_4 , filtered and finally evaporated to dryness. The resulting crude product was purified over Bio-Beads[®] S-X3 stationary phase and using THF as eluent. Ethynyl-functionalized thienyl-DPP **1** was obtained as a dark pink solid (29.5 mg, 54 μmol , yield 90%). $R_f = 0.38$ ($\text{CH}_2\text{Cl}_2/\text{heptane}$ 7 : 3, v/v); $^1\text{H NMR}$ (300 MHz, CDCl_3): δ 8.92 (dd, $^3J = 4.1$ Hz, $^4J = 1.2$ Hz, 1H), 8.79 (d, $^3J = 4.1$ Hz, 1H), 7.65 (dd, $^3J = 5.0$ Hz, $^4J = 1.2$ Hz, 1H), 7.38 (d, $^3J = 4.1$ Hz, 1H), 7.30-7.27 (m, 1H), 4.01 (m, 4H), 3.58 (s, 1H), 1.85 (m, 2H), 1.46-1.10 (m, 16H), 0.87 (m, 12H). Other spectroscopic data are identical to those reported by Yu *et al.*[58]

2.2.2 Unsymmetrical phenyl-DPP *N,N'*-TEG (**3**)

To a suspension of unsymmetrical phenyl-DPP pigment **2**[59] (703 mg, 1.91 mmol, 1.0 equiv), tetrabutylammonium chloride (TBACl, 27.0 mg, 97.0 μmol , 0.05 equiv) and K_2CO_3 (1.45 g, 10.5 mmol, 5.5 equiv) in DMF (15.5 mL), 1-chloro-2-(2-(2-methoxyethoxy)ethoxy)ethane[62] (3.50 g, 19.1 mmol, 10.0 equiv) was added dropwise, at 120 $^\circ\text{C}$ and under argon. The resulting reaction mixture was heated at 120 $^\circ\text{C}$ overnight. Thereafter, deionized water (21 mL) was added and the solution was filtered over a dicalite 4158 pad and washed with CHCl_3 until the filtrate was not fluorescent anymore. The aqueous layer was extracted four times with CHCl_3 . The combined organic layers were washed with deionized water twice, dried over anhydrous MgSO_4 , filtered and finally evaporated to dryness. The product was recrystallized in EtOH and was obtained as an orange solid (370 mg, 0.56 mmol, yield 29%). $R_f = 0.62$ ($\text{CH}_2\text{Cl}_2/\text{acetone}$ 8 : 2, v/v); IR (ATR): ν 3060, 2872 (CH_2 , CH_3), 1670 ($\text{C}=\text{O}$), 1605, 1593, 1559, 1489, 1446, 1424, 1405, 1382, 1350, 1294, 1263, 1350, 1294, 1263, 1201, 1149, 1104, 1087 ($\text{C}-\text{O}-\text{C}$), 1067, 1056, 1016, 919, 838, 778, 763, 743, 732, 712, 688, 644; $^1\text{H NMR}$ (500 MHz, CDCl_3): δ 7.97 (m, 2H), 7.94 (d, $^3J = 8.5$ Hz, 2H), 7.67 (d, $^3J = 8.5$ Hz, 2H), 7.52 (m, 3H), 3.94 (t, $^3J = 5.5$ Hz, 2H), 3.90 (t, $^3J = 5.5$ Hz, 2H), 3.74 (m, 4H), 3.60-3.54 (m, 12H), 3.50 (m, 4H), 3.36 (s, 3H), 3.34 (s, 3H); $^{13}\text{C NMR}$ (126 MHz, CDCl_3):

δ 163.0 (2C), 149.6, 148.0, 132.2 (2C), 131.4, 131.1 (2C), 129.5 (2C), 129.0 (2C), 128.1, 127.0, 125.9, 109.9, 109.7, 72.1 (2C), 70.7 (6C), 69.1, 69.0, 59.2 (2C), 42.5, 42.2; LRMS (ESI, positive mode): $m/z = 659.2 [M + H]^+$ and $681.2 [M + Na]^+$, calcd for $C_{32}H_{40}BrN_2O_8^+$ 659.2.

2.2.3 TMS-ethynyl-functionalized phenyl-DPP *N,N'*-TEG (4)

To a solution of *para*-bromoaryl DPP derivative **3** (250 mg, 0.38 mmol, 1.0 equiv), $Pd_2(dba)_3$ (104 mg, 0.11 mmol, 0.3 equiv) and $AsPh_3$ (290 mg, 0.95 mmol, 2.5 equiv) in dry THF (50 mL) and kept under argon, dry TEA (12.5 mL) was added. The mixture was heated at 60 °C and trimethylsilylacetylene (214 μ L, 1.52 mmol, 4.0 equiv) was added. The resulting reaction mixture was kept at 60 °C overnight. According to TLC (CH_2Cl_2 /acetone 8 : 2, v/v, $R_f = 0.74$), the reaction was found to be not complete. Further equivalents of trimethylsilylacetylene (ca. 100 equiv) and $Pd_2(dba)_3$ (1.0 equiv) were added until the reaction was completed. Thereafter, CH_2Cl_2 and deionized water were added. The organic layer was collected and the aqueous layer was extracted thrice with CH_2Cl_2 . The combined organic layers were dried over anhydrous Na_2SO_4 , filtered and finally evaporated to dryness. The resulting crude product was purified by size-exclusion column chromatography over Bio-Beads[®] S-X3 stationary phase and using THF as eluent. Compound **4** was obtained as an orange solid (193 mg, 0.29 mmol, yield 75%). IR (ATR): ν 3062, 2872 (CH_2 , CH_3), 2154 ($C\equiv C$), 1670 ($C=O$), 1606, 1591, 1496, 1447, 1425, 1382, 1349, 1248 (Si- CH_3), 1199, 1088 (C-O-C), 1053, 952, 838 (Si- CH_3), 783, 760, 737, 716, 692, 661, 643, 608; 1H NMR (500 MHz, $CDCl_3$): δ 8.00-7.94 (m, 4H), 7.58 (d, $^3J = 8.5$ Hz, 2H), 7.51 (m, 3H), 3.93 (m, 4H), 3.73 (m, 4H), 3.58-3.53 (m, 12H), 3.49 (m, 4H), 3.35 (s, 3H), 3.34 (s, 3H), 0.26 (s, 9H); ^{13}C NMR (126 MHz, $CDCl_3$): δ 163.0 (2C), 149.5, 148.2, 132.3 (2C), 131.3, 129.5 (2C), 129.3 (2C), 128.9 (2C), 128.1, 127.9, 126.1, 110.1, 109.8, 104.6, 97.5, 72.1 (2C), 70.7 (6C), 69.1, 69.0, 59.1 (2C), 42.4, 42.2, 0.0 (3C); LRMS (ESI, positive mode): $m/z = 677.4 [M + H]^+$ and $699.4 [M + Na]^+$, calcd for $C_{37}H_{49}N_2O_8Si^+$ 677.3.

2.2.4 Ethynyl-functionalized phenyl-DPP *N,N'*-TEG (5)

To a solution of TMS-ethynyl derivative **4** (50 mg, 74.0 μ mol, 1.0 equiv) in acetone (4 mL) and deionized water (1 mL), solid CsF (112 mg, 740 μ mol, 10.0 equiv) was added. The resulting reaction mixture was stirred at RT for 48 h. Then, deionized water (100 mL) was added and the desired product was extracted thrice with CH_2Cl_2 . The combined organic layers were dried over

anhydrous Na₂SO₄, filtered and finally evaporated to dryness. The resulting crude product was purified over Bio-Beads[®] S-X3 stationary phase and using CHCl₃ as eluent. Ethynyl-functionalized phenyl-DPP derivative **5** was obtained as an orange solid (44 mg, 73 μmol, yield 98%). R_f = 0.61 (CH₂Cl₂/acetone 8 : 2, v/v); IR (ATR): ν 3235 (C≡C-H), 3060, 2922 (CH₂, CH₃), 2872 (CH₂, CH₃), 1670 (C=O), 1607, 1592, 1574, 1555, 1490, 1447, 1427, 1383, 1351, 1294, 1269, 1200, 1086 (C-O-C), 1056, 1019, 923, 843, 783, 756, 737, 714, 690, 647; ¹H NMR (500 MHz, CDCl₃): δ 8.00 (d, ³J = 8.5 Hz, 2H), 7.97 (m, 2H), 7.62 (d, ³J = 8.5 Hz, 2H), 7.52 (m, 3H), 3.93 (m, 4H), 3.74 (m, 4H), 3.60-3.52 (m, 12H), 3.49 (m, 4H), 3.35 (s, 3H), 3.34 (s, 3H), 3.22 (s, 1H); ¹³C NMR (126 MHz, CDCl₃): δ 163.0 (2C), 149.7, 148.0, 132.5 (2C), 131.4, 129.5 (2C), 129.4 (2C), 128.9 (2C), 128.3, 128.0, 124.9, 110.2, 109.7, 83.3, 79.8, 72.0 (2C), 70.7 (5C), 69.0, 68.9, 59.1 (2C), 42.4, 42.2, 29.8; LRMS (ESI, positive mode): m/z = 605.3 [M + H]⁺ and 627.3 [M + Na]⁺, calcd for C₃₄H₄₁N₂O₈⁺ 605.3.

2.2.5 Pinacol boronate-functionalized phenyl-DPP N,N'-TEG (**6**)

To a solution of *para*-bromoaryl DPP derivative **3** (50 mg, 76 μmol, 1.0 equiv), PdCl₂(PPh₃)₂ (8 mg, 11.4 μmol, 0.15 equiv) and KOAc (30 mg, 304 μmol, 4.0 equiv) in 1,4-dioxane (5 mL), bis(pinacolato)diboron (29 mg, 114 μmol, 1.5 equiv) was added. The mixture was refluxed under argon for 4 h. Thereafter, deionized water (20 mL) was added and the solution was filtered over a dicalite 4158 pad and washed with CH₂Cl₂ until the filtrate was not fluorescent anymore. The aqueous layer was extracted thrice with CH₂Cl₂. The combined organic layers were washed with brine, dried over anhydrous Na₂SO₄, filtered and finally evaporated to dryness. The resulting crude product was purified by size-exclusion column chromatography over Bio-Beads[®] S-X3 stationary phase and using CHCl₃ as eluent. Pinacol boronate-functionalized phenyl-DPP derivative **6** was obtained as an orange solid (49 mg, 69.3 μmol, yield 92%). R_f = 0.62 (CH₂Cl₂/acetone 8 : 2, v/v); IR (ATR): ν 2870 (CH₂, CH₃), 1673 (C=O), 1605, 1592, 1492, 1448, 1356 (B-C), 1272, 1198, 1140, 1085 (C-O-C), 1019, 962, 929, 855, 786, 768, 752, 731, 696, 655; ¹H NMR (500 MHz, CHCl₃): δ 7.99-7.89 (m, 6H), 7.54-7.48 (m, 3H), 3.94 (m, 4H), 3.72 (t, ³J = 5.7 Hz, 2H), 3.70 (t, ³J = 5.7 Hz, 2H), 3.58-3.52 (m, 12H), 3.49 (m, 4H), 3.35 (s, 3H), 3.34 (s, 3H), 1.36 (s, 12H); ¹³C NMR (126 MHz, CDCl₃): δ 162.9 (2C), 149.4, 148.8, 135.1 (2C), 131.2, 130.5, 129.4 (2C), 128.8 (2C), 128.3 (2C), 128.1, 110.0, 109.7, 84.1 (2C), 72.0 (2C), 70.6 (6C), 68.9 (2C), 59.1 (2C), 42.0

(2C), 24.9 (4C); LRMS (ESI, positive mode): $m/z = 707.4 [M + H]^+$ and $729.4 [M + Na]^+$, calcd for $C_{38}H_{52}BN_2O_{10}^+$ 707.4.

2.2.6 Symmetrical phenyl-DPP *N,N'*-TEG (7)

To a suspension of 3,6-diphenyl-DPP pigment[60] (100 mg, 0.35 mmol, 1.0 equiv), TBACl (5.0 mg, 17.3 μ mol, 0.05 equiv) and K_2CO_3 (264 mg, 1.91 mmol, 5.5 equiv) in DMF (5 mL), 1-chloro-2-(2-(2-methoxyethoxy)ethoxy)ethane[60] (633 mg, 3.47 mmol, 10.0 equiv) was added dropwise, at 120 °C and under argon. The resulting reaction mixture was heated at 120 °C overnight. Thereafter, deionized water (10 mL) was added and the solution was filtered over a dicalite 4158 pad and washed with CH_2Cl_2 until the filtrate was not fluorescent anymore. The aqueous layer was extracted with CH_2Cl_2 twice. The combined organic layers were washed with brine, dried over anhydrous Na_2SO_4 , filtered and finally evaporated to dryness. The product was purified by silica gel column chromatography using a step gradient of acetone in CH_2Cl_2 as eluent (from 0% to 20%). Compound **7** was obtained as an orange solid (27 mg, 46.5 μ mol, yield 13%). $R_f = 0.59$ (CH_2Cl_2 /acetone 8 : 2, v/v); IR (ATR): ν 3057, 2966, 2912, 2868, 2804 (CH_2 , CH_3), 1667 (C=O), 1606, 1592, 1567, 1498, 1473, 1446, 1385, 1369, 1359, 1324, 1304, 1271, 1242, 1197, 1158, 1134, 1089 (C-O-C), 1036, 1021, 1001, 984, 927, 892, 863, 851, 840, 792, 764, 743, 722, 690, 637; 1H NMR (500 MHz, $CHCl_3$): δ 7.98-7.93 (m, 4H), 7.53-7.48 (m, 6H), 3.93 (t, $^3J = 5.7$ Hz, 4H), 3.72 (t, $^3J = 5.7$ Hz, 4H), 3.57-3.53 (m, 12H), 3.49-3.46 (m, 4H), 3.33 (s, 6H); ^{13}C NMR (126 MHz, $CDCl_3$) δ 163.0 (2C), 149.1 (2C), 131.2 (2C), 129.4 (4C), 128.9 (4C), 128.2 (2C), 109.7 (2C), 72.0 (2C), 70.7 (6C), 68.9 (2C), 59.1 (2C), 42.1 (2C); LRMS (ESI, positive mode): $m/z = 581.3 [M + H]^+$ and $603.3 [M + Na]^+$, calcd for $C_{32}H_{41}N_2O_8^+$ 581.3.

2.3 Synthesis of BC-DPP energy transfer triads

2.3.1 Synthesis of BC-DPP-1

3,13-Dibromo-5-methoxy-8,8,18,18-tetramethylbacteriochlorin **diBr-BC**[57] (10 mg, 18.3 μ mol, 1.0 equiv), $Pd_2(dba)_3$ (10 mg, 11.0 μ mol, 0.6 equiv) and $AsPh_3$ (28 mg, 91.3 μ mol, 5.0 equiv) were placed in a 25 mL two-neck round-bottom flask and three vacuum-argon cycles were performed. Dry THF (4 mL) and TEA (4 mL) were sequentially added and the mixture was heated at 60 °C. Then, a solution of ethynyl-functionalized thienyl DPP **1** (24 mg, 44 μ mol, 2.4 equiv) in

dry THF (4 mL) was added dropwise over 1 h. The resulting reaction mixture was stirred at 60 °C and under argon overnight. The solution was cooled to RT and aq. saturated NH₄Cl was added. The desired product was extracted thrice with CH₂Cl₂. The combined organic layers were dried over anhydrous Na₂SO₄, filtered over a dicalite 4158 pad and the filtrate was evaporated to dryness. The resulting crude residue was purified by size-exclusion column chromatography over Bio-Beads[®] S-X3 stationary phase and using THF as eluent. The product was washed with MeOH to remove 2,6-di-*tert*-butyl-4-methylphenol (BHT, stabilizer in THF). Bacteriochlorin-DPP hybrid **BC-DPP-1** was obtained as a dark-purple solid (10.6 mg, 7.1 μmol, yield 39%). ¹H NMR (500 MHz, CDCl₃): δ 9.10 (d, ³J = 4.0 Hz, 1H), 9.03 (d, ³J = 4.0 Hz, 1H), 8.95 (dd, ³J = 4.0 Hz, ⁴J = 1.2 Hz, 2H), 8.85 (s, 1H), 8.81 (d, ⁴J = 2.2 Hz, 1H), 8.78 (d, ⁴J = 2.2 Hz, 1H), 8.55 (s, 1H), 8.53 (s, 1H), 7.70 (d, ³J = 4.0 Hz, 1H), 7.66 (m, 3H), 7.30 (m, 2H), 4.49 (s, 3H), 4.43 (s, 4H), 4.11 (m, 8H), 2.11-2.00 (m, 4H), 1.96 (2s, 12H), 1.50-1.34 (m, 32H), 0.96-0.87 (m, 24H), -1.35 (s, 1H), -1.55 (s, 1H); ¹³C NMR (126 MHz, CDCl₃): *quantity isolated was too small for visualization of all carbon peaks, despite of extended acquisition time on a 500 MHz spectrometer equipped with a BBI probe (four times more sensitive in carbon than a standard 300 MHz spectrometer)*; LRMS (MALDI-TOF, positive mode): *m/z* = 1492.5 [M]⁺, calcd for C₈₉H₁₀₄N₈O₅S₄ 1492.7; HRMS (MALDI-TOF, positive mode): *m/z* = 1492.7085 [M]⁺, calcd for C₈₉H₁₀₄N₈O₅S₄ 1492.7007; LRMS (ESI, positive mode, cone voltage 200 V): *m/z* = 1492.9 (55), 1493.9 (100), 1496.0 (50) and 1497.0 (30) [M]⁺, calcd for C₈₉H₁₀₄N₈O₅S₄ 1492.7.

2.3.2 Synthesis of **BC-DPP-2**

BC-DPP-2 was synthesized following the same procedure as described for **BC-DPP-1** except that the product was washed with pentane to remove BHT. Ethynyl-functionalized phenyl-DPP *N,N'*-TEG **5** was used as starting material. Bacteriochlorin-DPP hybrid **BC-DPP-2** was obtained as a dark-red solid (3 mg, 1.9 μmol, yield 10%). ¹H NMR (500 MHz, CDCl₃): δ 8.91 (s, 1H), 8.82 (d, ⁴J = 2.2 Hz, 1H), 8.81 (d, ⁴J = 2.2 Hz, 1H), 8.56 (s, 1H), 8.54 (s, 1H), 8.21 (m, 4H), 8.03-8.00 (m, 8H), 7.55 (m, 6H), 4.51 (s, 3H), 4.44 (m, 4H), 4.07-3.99 (m, 8H), 3.84 (m, 4H), 3.79 (m, 4H), 3.66-3.63 (m, 12H), 3.59 (m, 8H), 3.58-3.55 (m, 8H), 3.53-3.51 (m, 4H), 3.40 (2s, 6H), 3.37 (2s, 6H), 1.97 (2s, 12H), -1.42 (s, 1H), -1.62 (s, 1H); ¹³C NMR (126 MHz, CDCl₃): *quantity isolated was too small for visualization of all carbon peaks, despite of extended acquisition time on a 500 MHz spectrometer equipped with a BBI probe (four times more sensitive in carbon than a standard*

300 MHz spectrometer); LRMS (MALDI-TOF, positive mode): $m/z = 1604.4 [M]^+$, calcd for $C_{93}H_{104}N_8O_{17}$ 1604.8; HRMS (MALDI-TOF, positive mode): $m/z = 1604.7496 [M]^+$, calcd for $C_{93}H_{104}N_8O_{17}$ 1604.7514; LRMS (ESI, positive mode, cone voltage 200 V): $m/z = 1605.9$ (90), 1606.9 (100) and 1608.1 (60) $[M + H]^+$, calcd for $C_{93}H_{105}N_8O_{17}^+$ 1605.8.

2.3.3 Synthesis of **BC-DPP-3**

diBr-BC (9 mg, 16.5 μ mol, 1.0 equiv), pinacol boronate-functionalized phenyl-DPP **6** (28 mg, 39.5 μ mol, 2.4 equiv), $PdCl_2(PPh_3)_2$ (2.5 mg, 3.3 μ mol, 0.2 equiv), PPh_3 (1.5 mg, 4.9 μ mol, 0.3 equiv) and K_2CO_3 (23 mg, 165 μ mol, 10.0 eq) were placed in a 10 mL two-neck round-bottom flask and three vacuum-argon cycles were performed. Dry toluene (3 mL) and dry DMF (1.5 mL) and the mixture was heated at 85 °C overnight. The mixture was then diluted with CH_2Cl_2 and deionized water was added. The product was extracted thrice with CH_2Cl_2 . The combined organic layers were washed twice with brine, dried over anhydrous Na_2SO_4 , filtered and finally evaporated to dryness. The resulting crude residue was purified by size-exclusion column chromatography over Bio-Beads[®] S-X3 stationary phase and using THF as eluent. The product was washed with pentane to remove BHT. Bacteriochlorin-DPP hybrid **BC-DPP-3** was obtained as a dark-orange solid (2 mg, 1.3 μ mol, yield 8%). 1H NMR (500 MHz, $CDCl_3$): δ 8.87 (s, 1H), 8.83 (s, 1H), 8.68-8.64 (m, 2H), 8.43 (d, $^3J = 8.1$ Hz, 2H), 8.36 (d, $^3J = 8.1$ Hz, 2H), 8.30 (d, $^4J = 2.0$ Hz, 3H), 8.05 (m, 4H), 7.59-7.51 (m, 8H), 4.43 (s, 2H), 4.39 (s, 2H), 4.17 (m, 3H), 4.06-4.02 (m, 4H), 3.93 (t, $^3J = 5.8$ Hz, 3H), 3.89 (t, $^3J = 5.8$ Hz, 3H), 3.83 (q, $^3J = 5.8$ Hz, 4H), 3.71 (s, 4H), 3.68-3.59 (m, 24H), 3.54-3.48 (m, 12H), 3.37 (s, 6H), 3.28 (s, 2H), 3.25 (s, 2H), 1.99 (d, $^3J = 7.0$ Hz, 8H), -1.50 (s, 1H), -1.75 (s, 1H); ^{13}C NMR (126 MHz, $CDCl_3$): *quantity isolated was too small for visualization of all carbon peaks, despite of extended acquisition time on a 500 MHz spectrometer equipped with a BBI probe (four times more sensitive in carbon than a standard 300 MHz spectrometer)*; HRMS (MALDI-TOF, positive mode): $m/z = 1556.7459 [M]^+$, calcd for $C_{89}H_{104}N_8O_{17}$ 1556.7514; LRMS (ESI, positive mode, cone voltage 200 V): $m/z = 1557.8$ (40), 1558.9 (40) and 1560.0 (20) $[M + H]^+$, calcd for $C_{89}H_{105}N_8O_{17}^+$ 1557.8.

3. Results and discussion

A survey of the literature related to hydroporphyrin-containing dyads clearly shows that the preferred strategy to readily access to these NIR-emissive two-component arrays is often based on

Pd-catalyzed cross-coupling reactions (typically, Sonogashira or Suzuki-Miyaura-type reactions)[53,55,63-65], even if other methods such as amide coupling and oxidative dimerization have been occasionally implemented[52,66,67]. This has been particularly useful in diversifying structure of the bridging unit between the two chromophores, and thus altering the electronic and photophysical properties of the resulting dyad. Since these coupling chemistries are versatile, reliable and well-mastered, synthetic difficulties are often associated only with the preparation of selected monomeric photoactive building blocks to covalently link together and/or the purification of the resulting hydroporphyrin-based conjugates. The availability of a set of orthogonal reactive functional groups within the core structure of coupling partners, required for both synthesis and fine-tuning the properties of these multi-chromophore systems, is a prerequisite, easier to achieve with small molecule fluorophores structurally simpler than (bacterio)chlorins. In this context, we opted for 3,6-diaryl-substituted DPP derivatives as fluorescent organic dyes spectrally compatible with bacteriochlorins and easily derivatizable platform molecules for rapid and effective post-synthetic functionalization of the targeted hybrid NIR fluorophores. This choice was supported by the recent and valuable advances in the chemistry of DPP-based fluorescent probes for applications in analyte sensing and molecular imaging[49,50]. Indeed, they highlight effective and easily implementable synthetic methodologies for the site-specific introduction of various chemical moieties including reporters, water-solubilizing groups and targeting ligands onto the DPP scaffold. Furthermore, it is well established that the simple replacement of 3,6-phenyl substituents by aromatic five-membered ring heteroaryl groups (typically, furyl or thienyl) leads to significant and desirable changes in their optical properties (*e.g.*, bathochromic shift of absorption/emission maxima, stronger charge transfer and larger two-photon absorption cross-sections). For the synthesis of first BC-DPP conjugates, assumed as model compounds to obtain a proof-of-concept for this novel class of hybrid NIR fluorophores, we have chosen to work with 3,6-diphenyl- and 3,6-dithienyl-substituted DPP dyes. Further introduction of branched alkyl (*i.e.*, 2-ethylhexyl groups) or oligoethylene glycol side-chains attached onto the *N*-positions of their lactam moieties was also planned in order to enhance the solubility of the DPP-based coupling partners in a wide range of organic solvents (Fig. 2). Interestingly, in the field of DPP-based conjugated polymers for bulk heterojunction solar cells, solubilizing chains play a critical role on the efficiency of the material. In particular, the 2-ethylhexyl group was found well-adapted as short bulky branched

chain to form films with suitable morphology leading to higher carrier mobility, and the synthesis of DPP derivative **1** has already been regarded in this context, especially by us[68,69].

Synthetic routes devised for preparing the 3,6-diphenyl-DPP dyes and installing the reactive functional group required for their covalent conjugation to 3,13-dibromo-5-methoxy-8,8,18,18-tetramethylbacteriochlorin[57] **diBr-BC** (*i.e.*, terminal alkyne for Sonogashira-type coupling and pinacol boronate ester for Suzuki-Miyaura reaction)[70] are first discussed. Emphasis is next placed on the optimization of both Pd-catalyzed cross-coupling reactions between these "ready-to-use" functionalized DPP derivatives and **diBr-BC** and purification protocols of the hybrid fluorophores obtained. Finally, fluorescence behavior of BC-DPP triads in solution, especially in the NIR range, is studied in details.

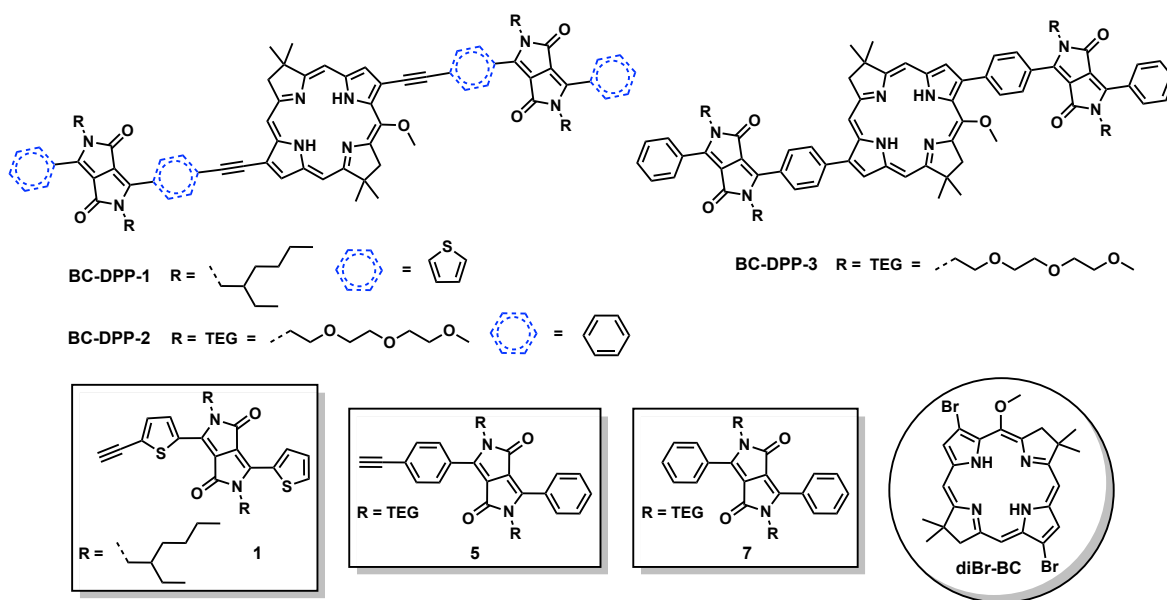
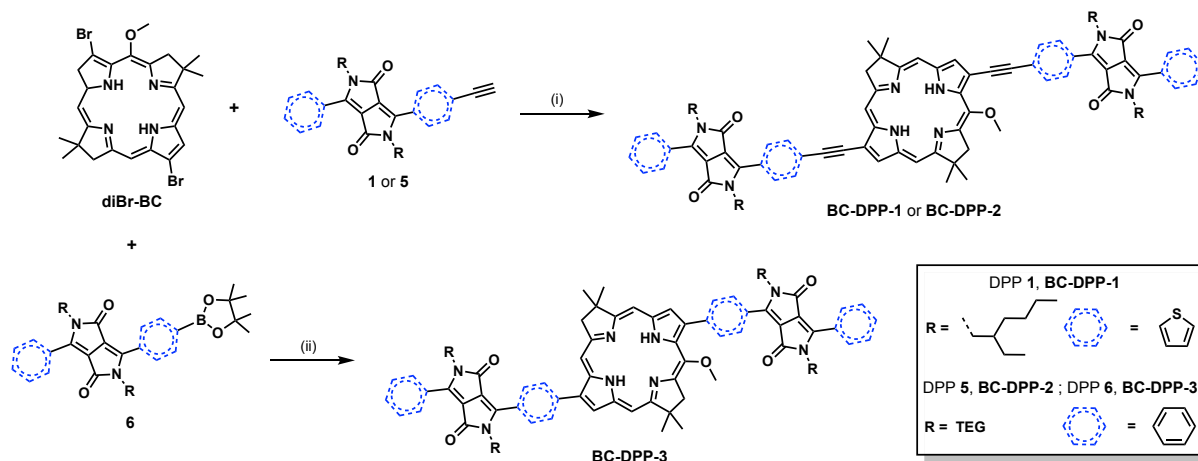


Fig. 2. Structures of DPP dyes and BC-DPP triads studied in this work.

3.1 Synthesis of "ready-to-use" functionalized DPP derivatives

The synthetic routes used to prepare the 3,6-diphenyl-DPP derivatives functionalized either with a pinacol boronate ester or a terminal alkyne are depicted in Scheme 1. The common starting unsymmetrical DPP pigment **2** was prepared according to literature procedures.[59] *N*-Alkylation of its lactam moieties was performed using an excess of 1-chloro-2-(2-(2-methoxyethoxy)ethoxy)ethane and under phase-transfer conditions to give organic-soluble DPP dye **3** in modest 29% yield. Short oligo(ethyleneglycol) moieties (abbreviated here TEG) were

chosen as *N*-substituents to partially counterbalance the assumed great hydrophobicity of BC-DPP conjugates and thus considering spectral and photophysical measurements in solution conditions that limit or prevent aggregate formation. Copper-free Sonogashira cross-coupling reaction (also known as Heck alkynylation) between **3** and trimethylsilylacetylene provided the compound **4** in good 75% yield. In our optimizations of this Pd-catalyzed alkynylation, very sensitive precatalysts and ligands were avoided, the objective being to develop very simple, reliable and robust conditions. Therefore, we have chosen to use the air-stable Pd₂(dba)₃ with triphenylarsine as a dative ligand[71]. AsPh₃ is a relatively inexpensive ligand that is easy to handle, and stable in air. It is also important to specify that all our attempts to purify TMS-protected alkyne **4** by conventional column chromatography over regular silica gel failed. Conversely, we found that the use of a styrene-divinylbenzene gel with a pore size of 50 Å and an exclusion limit of 2000 Da (Bio-Beads[®] S-X3), was particularly effective to recover this functionalized-DPP in a pure form, through size-exclusion chromatography process. Final step toward ethynyl-functionalized phenyl-DPP dye **5** involved the deprotection of TMS group. Once again, optimization of the reaction conditions was required because the use of conventional source of fluoride anions (*i.e.*, TBAF) led to degradation of the functionalized DPP dye. Furthermore, alkaline deprotection with K₂CO₃ was found to be relatively ineffective because a major amount of starting compound was recovered after 12 h of reaction. Finally, the use of cesium fluoride (CsF) in an acetone-H₂O mixture led to quantitative removal of the TMS group[72] and the resulting terminal alkyne was easily purified by size-exclusion chromatography.



Scheme 2. Synthetic routes toward DPP-BC triads. *Reagents and conditions:* (i) Pd₂(dba)₃, AsPh₃, TEA, THF, 60 °C, Ar atmosphere, overnight, yield 39% (**BC-DPP-1**) and 10% (**BC-DPP-2**); (ii) Pd(PPh₃)₂Cl₂, PPh₃, K₂CO₃, toluene-DMF (1 : 1, v/v), 85 °C, Ar atmosphere, overnight, yield 8% (**BC-DPP-3**).

With ethynyl-functionalized DPP derivatives **1** and **5** as the starting material, the copper-free Sonogashira cross-coupling reaction with **diBr-BC** worked properly using Pd₂(dba)₃/AsPh₃ as catalyst system, in a TEA-THF mixture at 60 °C. However, it is important to point out that the success of this Pd-catalyzed heterocoupling greatly depend on the purity level of **diBr-BC** that must be isolated with the utmost care. The resulting high-molecular photoactive molecular triads **BC-DPP-1** and **BC-DPP-2** were readily purified by size-exclusion chromatography, using the same resin as that employed for isolation of functionalized DPP derivatives (*vide supra*). Moderate to low yields (39% and 10% respectively) are partly due material losses inherent to the small scale of syntheses (ca. 20 μmol of **diBr-BC**, the limiting starting material). Gratifyingly, the Suzuki-Miyaura cross-coupling between pinacol boronate ester **6** and **diBr-BC** was found to work under standard conditions to afford after purification by size-exclusion chromatography the triad **BC-DPP-3** in 8% yield.

The three BC-DPP triads were fully characterized by ¹H NMR and low- and high-resolution mass spectrometry (see ESI for the corresponding spectra, Fig. S22-S32). Spectroscopic data were in agreement with the structures assigned. In particular, ¹H NMR spectrum of each triad shows a set of proton resonance signals that can be assumed as the overall sum of ¹H NMR spectra of its chromophoric units (BC and 2 × DPP), even if some aromatic protons' signals of DPP scaffold spatially close to the bacteriochlorin π framework are significantly shifted downfield in comparison with the parent DPP derivative (*e.g.*, doublet assigned to one thienyl proton of **1** is shifted from 7.38 to 7.70 ppm, doublet assigned to two phenyl protons of **5** is shifted from 7.62 to 8.00 ppm,

see ESI for the corresponding NMR spectra, Fig. S1, S11, S22 and S26). Since these polycyclic aromatic molecules are assumed to be poorly ionizable, MALDI was the preferred ionization method for their facile mass analysis (both low- and high-resolution). However, we also explored the feasibility of performing these mass spectrometry characterizations by ESI and we found that the tuning of cone voltage parameter (200 V instead of 75 V, typical value for the MSQ mass spectrometer currently used by us) allowed to obtain also good-quality mass spectra in the positive mode (see ESI for the corresponding mass spectra, Fig. S25, S29, and S32).

3.3 Photophysical properties of BC-DPP triads

The photophysical properties of bacteriochlorin-based triads as well as parent monomeric chromophores were evaluated in weakly polar solvents namely CHCl_3 and toluene, with a choice being made according to solubility criteria. Absorption and emission properties are gathered in Tables 1 and 2, and selected examples of spectra of **BC-DPP-2** and **BC-DPP-3** are available in Fig. 3 (see ESI for the other absorption/excitation/emission spectra, Fig. S33-S52). As expected, the UV-vis absorption spectra are essentially the sum of those of DPP and bacteriochlorin scaffolds as revealed by a set of maxima assigned to B (in the range 357-375 nm), Q_x (in the range 515-533 nm), Q_y (in the range 746-795 nm) bands of hydroporphyrin and $S_0 \rightarrow S_1$ band of energy donor (in the range 482-593 nm). Effect of both distinct solvents on these electronic absorption spectra is not really significant (Table 2, columns 3 and 4). Interestingly, the simultaneous substitution of 3,13-positions of bacteriochlorin macrocycle by ethynyl or phenyl moieties causes a dramatic bathochromic shift of the Q_y band within the NIR range (+72 nm, +45 nm, +23 nm for **BC-DPP-1**, **BC-DPP-2** and **BC-DPP-3** respectively and compared to **diBr-BC**, +86 nm, +59 nm and +37 nm compared to **BC[57]**).

Table 1. Absorption and emission properties of **diBr-BC** and DPP monomers in selected organic solvents.

Fluorophore	Solvent	Abs λ_{max} (nm)	ϵ ($\text{M}^{-1} \text{cm}^{-1}$)	Em λ_{max} (nm)	Φ_{F} (%) ^a
diBr-BC ^b	CHCl_3	350, 355, 371, 505, 723	91 700,	non-fluorescent	non-fluorescent
			85 350,		
			90 300,		
			29 650,		
			94 550		

diBr-BC	toluene	351, 358, 371, 506, 723	82 450, 81 400, 86 300, 29 300, 95 255	non- fluorescent	non-fluorescent
1	CHCl ₃	530, 568	18 475, 20 350	587, 637	55
1	toluene	532, 573	22 950, 27 400	588, 642	77
5	CHCl ₃	475	16 200	539 ^c	100
5	toluene	479	16 350	546 ^c	95
7	CHCl ₃	470	21 750	522 ^c	89
7	toluene	470	20 270	528 ^c	88

^a Fluorescence quantum yields were determined at 25 °C by a relative method using the following standards[73]: sulforhodamine 101 (SR101, $\Phi_F = 95\%$ in EtOH) for DPP dye **1** and fluorescein ($\Phi_F = 90\%$ in 0.1 M NaOH) for DPP dyes **5** and **7**.

^b Absorption maximum (Q_y band) of parent non-brominated bacteriochlorin is 709 nm in CH₂Cl₂[57].

^c Shoulder peak was observed on the emission spectrum: around 570 nm and 580 nm for **5** in CHCl₃ and toluene respectively; 550 nm and 560 nm for **7** in CHCl₃ and toluene respectively.

It should be borne in mind that the relative large width and poorly structured shape noted for B band are the result of an overlay with S₀→S₂ band of DPP chromophore, not electronic interactions between the two distinct fluorophore units in the ground state. Indeed, the ethynyl linker (for triads **BC-DPP1** and **BC-DPP-2**) or the connecting phenyl moiety (for triad **BC-DPP-3**) prevents the donors and acceptor fragments from becoming planar and thus extended π -electronic conjugation. Excitation at each absorption band of the triads results in an emission in the NIR spectral window (Table 2, column 5 for the corresponding emission maxima depending upon triad and solvent).

Table 2. Absorption and emission properties of BC-DPP triads and published BC-BODIPY dyads, in selected organic solvents.

Dyad / Triad	Solvent	Abs λ_{\max} (nm)	ϵ (M ⁻¹ cm ⁻¹)	Em λ_{\max} (nm)	Φ_F (%) ^a	ETE (%) ^b
BC-DPP-1	CHCl ₃	364, 590, 795	102 600, 94 300, 132 760	811	7.5	98
BC-DPP-1	toluene	364, 593, 795	94 260, 95 770,	811	8	97

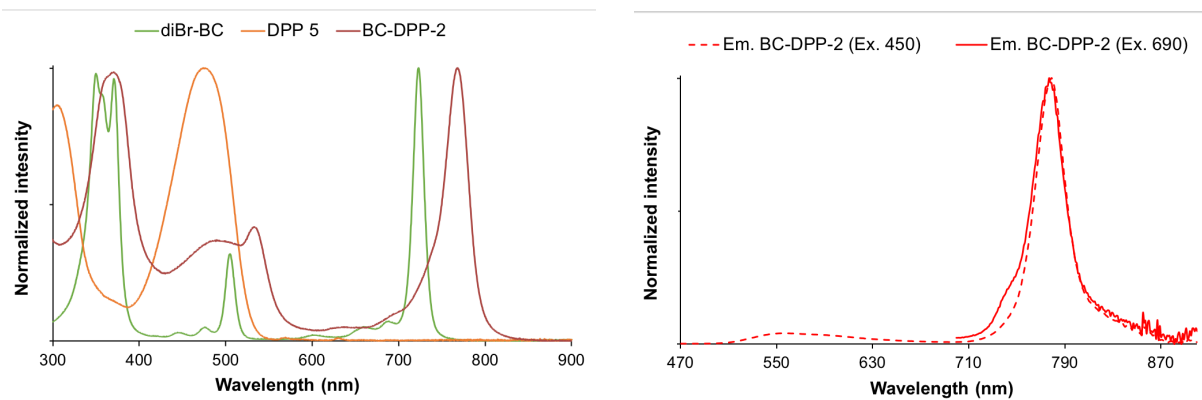
			128 900			
BC-DPP-2	CHCl ₃	370, 490, 533, 768	91 400, 34 300, 38 800, 92 970	779	11	99
BC-DPP-2	toluene	375, 490, 533, 768	89 450, 34 520, 43 700, 97 800	776	12	99
BC-DPP-3	CHCl ₃	358, 370, 482, 515, 746	67 180, 69 350, 24 360, 24 300, 47 420	761	6.5	96
BC-DPP-3	toluene	357, 370, 484, 517, 746	73 200, 73 200, 25 900, 29 400, 58 000	760	13	96
BC-BODIPY-1 _[55]	toluene	371, 504, 735	-	744	-	93
BC-BODIPY-2 _[65]	toluene	-, 505, 745	-	754	-	96

^a Fluorescence quantum yields were determined at 25 °C by a relative method using indocyanine green as standard (ICG, $\Phi_F = 10.6\%$ in DMSO, Ex. at their Q_y band: 720 nm, 690 nm and 680 nm for **BC-DPP-1**, **BC-DPP-2** and **BC-DPP-3** respectively)[73].

^b Energy transfer efficiency was calculated based on the equation $\{100 \times [1 - (\Phi_F \text{ donor in triad})/(\Phi_F \text{ free donor})]\}$. The following DPP dyes were used as free donors: **1** for **BC-DPP-1** (Ex. at 550 nm, Em. 560-725 nm), **5** for **BC-DPP-2** (Ex. at 450 nm, Em. 470-710 nm) and **7** for **BC-DPP-3** (Ex. 450 nm, Em. 470-710 nm).

Emission spectra displayed in Fig. 3 and Fig. S40, S42, S44 and S46 clearly illustrate the ability of the DPP parts of these triads to transfer energy to the bacteriochlorin moiety. This was also supported by the excitation spectra that perfectly match with the absorption curves of the triads (see Fig. S47-S52). Energy transfer efficiency, calculated based on the equation $\{100 \times [1 - (\Phi_F \text{ donor in triad})/(\Phi_F \text{ free donor})]\}$ exceeds 96% for each triad (Table 2, column 6). The sole difficulty associated with these measurements, was to find both an appropriate excitation wavelength of DPP donors for which the residual absorption of bacteriochlorin (*i.e.*, Q_x band) was negligible and an emission spectral range for DPP dye not hindered by NIR emission of BC

acceptor (see caption of Table 2 and ESI for experimental details). These results thus indicate that DPP dyes are efficient donors to bacteriochlorins and the ethynyl moiety is a proper twisted conjugate linker to promote energy transfer between these donor and acceptor units. Interestingly, three-chromophore systems such as triads **BC-DPP-1-3** enable to achieve large pseudo-Stokes shift upon excitation in the blue-green region: 260 nm ($5\,850\text{ cm}^{-1}$) for **BC-DPP-1** (Ex. at 550 nm) and 310-330 nm ($9\,065\text{ cm}^{-1}$ - $9\,385\text{ cm}^{-1}$) for **BC-DPP-2-3** (Ex. at 450 nm). This spectral behavior is quite similar to that of some bacteriochlorin-BODIPY dyads recently published by the Ptaszek group (see Fig. 4 and Table 2, entries 7-8). Indeed, excitation at the maximum of BODIPY absorbance (*ca.* 500 nm) resulted in nearly exclusive NIR emission of bacteriochlorin component (744-754 nm). A slight difference in ETE values was obtained in view of the nature of linker connecting the two chromophoric units (93% with phenylene and 96% with phenylacetylene). Finally, satisfactory values of fluorescence quantum yields, in the range 6-13%, were obtained upon direct excitation of the triads at their Q_y band. These emission features associated with attractive red-shifted absorption properties in the range 745-795 nm (*vide supra*), are particular of interest for considering the forthcoming use of these triads as valuable building blocks in the rational design of NIR fluorophores for biomedical applications.



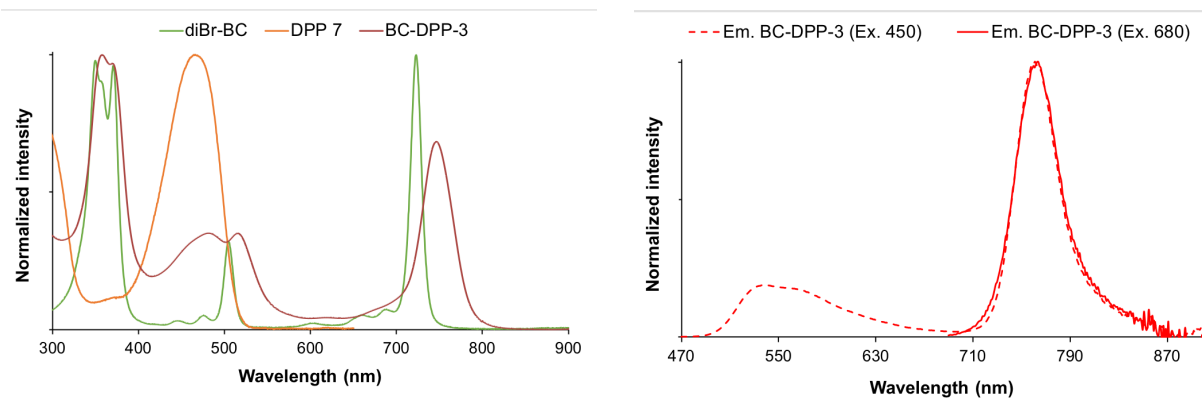


Fig. 3. Normalized absorption and emission spectra of BC-DPP triads in CHCl_3 at 25°C . (Top left) Overlay of the absorbance spectra of diBr-BC, DPP 5 and BC-DPP-2; (Top right) Overlay of the emission spectra of BC-DPP-2 upon excitation at 450 nm (slit 5 nm, Em. 470-900 nm, slit 5 nm) and 690 nm (slit 5 nm, Em. 700-900 nm, slit 5 nm); (Bottom left) Overlay of the absorbance spectra of diBr-BC, DPP 7 and BC-DPP-3; (Bottom right) Overlay of the emission spectra of BC-DPP-3 upon excitation at 450 nm (slit 5 nm, Em. 470-900 nm, slit 5 nm) and 680 nm (slit 5 nm, Em. 690-900 nm, slit 5 nm). Please note: emission spectra cannot be corrected in the range 850-900 nm, which explains the artifact observed at 850 nm.

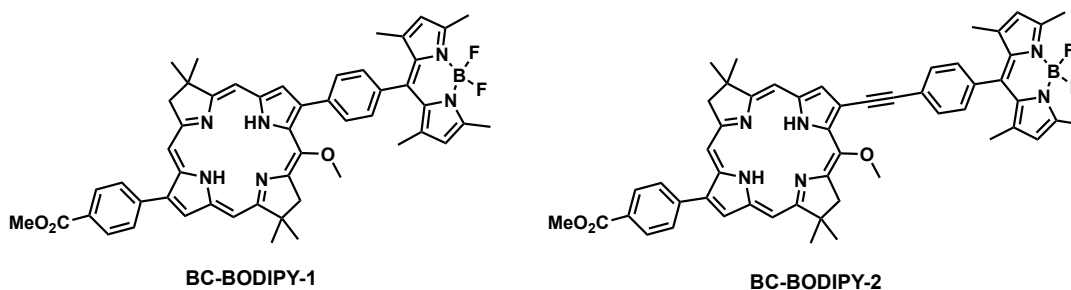


Fig. 4. Structures of BC-BODIPY dyads recently reported by the Ptaszek group[65,55].

4. Conclusion

In summary, unprecedented donor-acceptor-donor systems based on DPP dyes and a bioinspired porphyrin-like fluorophore were successfully synthesized for the first time, through concise and convergent synthetic routes. Very efficient energy transfer ($\text{ETE} > 96\%$) is observed from DPP to NIR absorbing bacteriochlorin, for two different DPP with absorption spanning 470-575 nm, and results in an intense emission within the "therapeutic optical window". Compared to energy transfer dyads involving a bacteriochlorin as acceptor, and already reported in the literature, the availability of DPP moieties within the core structure of these fluorescent molecular hybrids, offers a unique opportunity to easily tailor properties of hydroporphyrins for specific biomedical or energy-related applications. Indeed, these structurally compact chromophores possess an

unsurpassed range of valuable features including: straightforward synthesis, ease of modification, outstanding robustness (both (photo)chemical and thermal stability) and attractive spectroscopic properties[49,50]. In this context, site-specific functionalizations of DPP fragments with the aim of introducing some water-solubilizing groups, a bioconjugatable tether or an optically tunable group within the structure of triads is currently under investigation in our laboratory. Indeed, this will pave the way for a next generation of high-performance NIR-I fluorophores that will facilitate biosensing/bioimaging in complex biological systems.

Acknowledgments

This work is supported by the CNRS, Université de Bourgogne and Conseil Régional de Bourgogne through the "Plan d'Actions Régional pour l'Innovation (PARI)" and the "Fonds Européen de Développement Régional (FEDER)" programs, especially for post-doctoral fellowship of Dr. Pritam Mondal. Flavien Ponsot gratefully acknowledges the French Research Ministry for his Ph. D. grant. Financial support from Institut Universitaire de France (IUF), the Burgundy region ("FABER" programme, PARI Action 6, SSTIC 6 "Imagerie, instrumentation, chimie et applications biomédicales") and GDR CNRS "Agents d'Imagerie Moléculaire" (AIM) 2037 are also greatly acknowledged. The authors thank the "Plateforme d'Analyse Chimique et de Synthèse Moléculaire de l'Université de Bourgogne" (PACSMUB, <http://www.wpcm.fr>) for access to analytical instrumentation. COBRA lab (UMR CNRS 6014) and Iris Biotech company are warmly thanked for the generous gift of some chemical reagents used in this work. The authors also thank Mrs. Sandrine Pacquelet (University of Burgundy, ICMUB, UMR CNRS 6302), Mrs. Julie Mathey (student at the University Technology Institute in Besançon, 2017) and Mrs. Gracia Loma Kikobo (undergraduate student from the University of Burgundy, Dijon, 2018) for their technical assistance during the synthesis of **diBr-BC** and some DPP derivatives.

Appendix A. Supplementary data

Supplementary data related to this article can be found online at

References

- [1] Weissleder R, Mahmood U. *Molecular Imaging Radiology* 2001; 219: 316-33.
- [2] Pysz MA, Gambhir SS, Willmann JK. *Molecular imaging: current status and emerging strategies Clin. Radiol.* 2010; 65: 500-16.
- [3] Bremer C, Ntziachristos V, Weissleder R. *Optical-based molecular imaging: contrast agents and potential medical applications Eur. Radiol.* 2003; 13: 231-43.
- [4] Weissleder R, Ntziachristos V. *Shedding light onto live molecular targets Nat. Med.* 2003; 9: 123-8.
- [5] Frangioni JV. *In vivo near-infrared fluorescence imaging Curr. Opin. Chem. Biol.* 2003; 7: 626-34.
- [6] Rao J, Dragulescu-Andrasi A, Yao H. *Fluorescence imaging in vivo: recent advances Curr. Opin. Chem. Biol.* 2007; 18: 17-25.
- [7] Sevick-Muraca EM. *Translation of near-infrared fluorescence imaging technologies: emerging clinical applications Annu. Rev. Med.* 2012; 63: 217-31.
- [8] Pansare VJ, Hejazi S, Faenza WJ, Prud'homme RK. *Review of Long-Wavelength Optical and NIR Imaging Materials: Contrast Agents, Fluorophores, and Multifunctional Nano Carriers Chem. Mater.* 2012; 24: 812-27.
- [9] Hong G, Antaris AL, Dai H. *Near-infrared fluorophores for biomedical imaging Nat. Biomed. Eng.* 2017; 1: 0010, DOI: 10.1038/s41551-016-0010.
- [10] Martinić I, Eliseeva SV, Petoud S. *Near-infrared emitting probes for biological imaging: Organic fluorophores, quantum dots, fluorescent proteins, lanthanide(III) complexes and nanomaterials J. Lumin.* 2017; 189: 19-43.
- [11] Chan J, Dodani SC, Chang CJ. *Reaction-based small-molecule fluorescent probes for chemoselective bioimaging Nat. Chem.* 2012; 4: 973-84.
- [12] Grimm JB, Heckman LM, Lavis LD. *The chemistry of small-molecule fluorogenic probes Prog. Mol. Biol. Transl. Sci.* 2013; 113: 1-34.
- [13] Luby BM, Charron DM, MacLaughlin CM, Zheng G. *Activatable fluorescence: From small molecule to nanoparticle Adv. Drug Deliv. Rev.* 2017; 113: 97-121.
- [14] Ballou B, Ernst LA, Waggoner AS. *Fluorescence imaging of tumors in vivo Curr. Med. Chem.* 2005; 12: 795-805.
- [15] Ptaszek M. *Rational design of fluorophores for in vivo applications Prog. Mol. Biol. Transl. Sci.* 2013; 113: 59-108.
- [16] Umezawa K, Citterio D, Suzuki K. *New Trends in Near-Infrared Fluorophores for Bioimaging Anal. Sci.* 2014; 30: 327-49.
- [17] Kushida Y, Nagano T, Hanaoka K. *Silicon-substituted xanthene dyes and their applications in bioimaging Analyst* 2015; 140: 685-95.
- [18] Ikeno T, Nagano T, Hanaoka K. *Silicon-substituted Xanthene Dyes and Their Unique Photophysical Properties for Fluorescent Probes Chem. - Asian J.* 2017; 12: 1435-46.
- [19] Chen H, Dong B, Tang Y, Lin W. *A Unique "Integration" Strategy for the Rational Design of Optically Tunable Near-Infrared Fluorophores Acc. Chem. Res.* 2017; 50: 1410-22.
- [20] Ptaszek M, Kee H-L, Muthiah C, Nothdurft R, Akers W, Achilefu S, Culver JP, Holten D. *Near-infrared molecular imaging probes based on chlorin-bacteriochlorin dyads Proc. SPIE* 2010; 7576: 75760E/1-E/9.
- [21] Alexander VM, Sano K, Yu Z, Nakajima T, Choyke PL, Ptaszek M, Kobayashi H. *Galactosyl Human Serum Albumin-NMP1 Conjugate: A Near Infrared (NIR)-Activatable Fluorescence Imaging Agent to Detect Peritoneal Ovarian Cancer Metastases Bioconjugate Chem.* 2012; 23: 1671-9.
- [22] Harada T, Sano K, Sato K, Watanabe R, Yu Z, Hanaoka H, Nakajima T, Choyke PL, Ptaszek M, Kobayashi H. *Activatable Organic Near-Infrared Fluorescent Probes Based on a Bacteriochlorin Platform: Synthesis and Multicolor in Vivo Imaging with a Single Excitation Bioconjugate Chem.* 2014; 25: 362-9.
- [23] de Oliveira KT, Momo PB, de Assis FF, Ferreira MAB, Brocksom TJ. *Chlorins: Natural Sources, Synthetic Developments and Main Applications Curr. Org. Synth.* 2014; 11: 42-58.
- [24] Grin MA, Mironov AF. *Synthetic and natural bacteriochlorins: synthesis, properties and applications In: Chemical Processes with Participation of Biological and Related Compounds, Boca Raton: CRS Press; 2008, p. 5-43.*
- [25] Ruzi'c C, Krayner M, Balasubramanian T, Lindsey JS. *Tailoring a Bacteriochlorin Building Block with Cationic, Amphipathic, or Lipophilic Substituents J. Org. Chem.* 2008; 73: 5806-20.
- [26] Taniguchi M, Cramer DL, Bhise AD, Kee HL, Bocian DF, Holten D, Lindsey JS. *Accessing the near-infrared spectral region with stable, synthetic, wavelength-tunable bacteriochlorins New J. Chem.* 2008; 32: 947-58.

- [27] Kee HL, Diers JR, Ptaszek M, Muthiah C, Fan D, Lindsey JS, Bocian DF, Holten D. Chlorin-bacteriochlorin energy-transfer dyads as prototypes for near-infrared molecular imaging probes: controlling charge-transfer and fluorescence properties in polar media *Photochem. Photobiol.* 2009; 85: 909-20.
- [28] Lindsey JS, Mass O, Chen C-Y. Tapping the near-infrared spectral region with bacteriochlorin arrays *New J. Chem.* 2011; 35: 511-6.
- [29] Yang E, Kirmaier C, Krayner M, Taniguchi M, Kim H-J, Diers JR, Bocian DF, Lindsey JS, Holten D. Photophysical Properties and Electronic Structure of Stable, Tunable Synthetic Bacteriochlorins: Extending the Features of Native Photosynthetic Pigments *J. Phys. Chem. B* 2011; 115: 10801-16.
- [30] Jiang J, Chen C-Y, Zhang N, Vairaprakash P, Lindsey JS. Polarity-tunable and wavelength-tunable bacteriochlorins bearing a single carboxylic acid or NHS ester. Use in a protein bioconjugation model system *New J. Chem.* 2015; 39: 403-19.
- [31] Jiang J, Taniguchi M, Lindsey JS. Near-infrared tunable bacteriochlorins equipped for bioorthogonal labeling *New J. Chem.* 2015; 39: 4534-50.
- [32] Jiang J, Yang E, Reddy KR, Niedzwiedzki DM, Kirmaier C, Bocian DF, Holten D, Lindsey JS. Synthetic bacteriochlorins bearing polar motifs (carboxylate, phosphonate, ammonium and a short PEG). Water-solubilization, bioconjugation, and photophysical properties *New J. Chem.* 2015; 39: 5694-714.
- [33] Mandal AK, Sahin T, Liu M, Lindsey JS, Bocian DF, Holten D. Photophysical comparisons of PEGylated porphyrins, chlorins and bacteriochlorins in water *New J. Chem.* 2016; 40: 9648-56.
- [34] Liu R, Liu M, Hood D, Chen C-Y, MacNevin C, Holten D, Lindsey J. Chlorophyll-Inspired Red-Region Fluorophores: Building Block Synthesis and Studies in Aqueous Media *Molecules* 2018; 23: 130.
- [35] Kim H-J, Lindsey JS. De Novo Synthesis of Stable Tetrahydroporphyrinic Macrocycles: Bacteriochlorins and a Tetrahydrocorrin *J. Org. Chem.* 2005; 70: 5475-86.
- [36] Fan D, Taniguchi M, Lindsey JS. Regioselective 15-Bromination and Functionalization of a Stable Synthetic Bacteriochlorin *J. Org. Chem.* 2007; 72: 5350-7.
- [37] Liu Y, Lindsey JS. Northern-Southern Route to Synthetic Bacteriochlorins *J. Org. Chem.* 2016; 81: 11882-97.
- [38] Liu Y, Zhang S, Lindsey JS. Total synthesis campaigns toward chlorophylls and related natural hydroporphyrins - diverse macrocycles, unrealized opportunities *Nat. Prod. Rep.* 2018: in press, see DOI: 10.1039/c8np00020d.
- [39] For selected examples of porphyrin-DPP hybrids, see: Warnan J, Favereau L, Meslin F, Severac M, Blart E, Pellegrin Y, Jacquemin D, Odobel F. Diketopyrrolopyrrole-Porphyrin Conjugates as Broadly Absorbing Sensitizers for Dye-Sensitized Solar Cells *ChemSusChem* 2012; 5: 1568-77 and references [40-48].
- [40] Favereau L, Warnan J, Anne FB, Pellegrin Y, Blart E, Jacquemin D, Odobel F. Diketopyrrolopyrrole-zinc porphyrin, a tuned panchromatic association for dye-sensitized solar cells *J. Mater. Chem. A* 2013; 1: 7572-5.
- [41] Gao K, Li L, Lai T, Xiao L, Huang Y, Huang F, Peng J, Cao Y, Liu F, Russell TP, Janssen RAJ, Peng X. Deep Absorbing Porphyrin Small Molecule for High-Performance Organic Solar Cells with Very Low Energy Losses *J. Am. Chem. Soc.* 2015; 137: 7282-5.
- [42] Schmitt J, Heitz V, Sour A, Bolze F, Ftouni H, Nicoud J-F, Flamigni L, Ventura B. Diketopyrrolopyrrole-Porphyrin Conjugates with High Two-Photon Absorption and Singlet Oxygen Generation for Two-Photon Photodynamic Therapy *Angew. Chem., Int. Ed.* 2015; 54: 169-73.
- [43] Liang T, Xiao L, Liu C, Gao K, Qin H, Cao Y, Peng X. Porphyrin small molecules containing furan- and selenophene-substituted diketopyrrolopyrrole for bulk heterojunction organic solar cells *Org. Electron.* 2016; 29: 127-34.
- [44] Schmitt J, Heitz V, Sour A, Bolze F, Kessler P, Flamigni L, Ventura B, Bonnet CS, Toth E. A Theranostic Agent Combining a Two-Photon-Absorbing Photosensitizer for Photodynamic Therapy and a Gadolinium(III) Complex for MRI Detection *Chem. - Eur. J.* 2016; 22: 2775-86.
- [45] Sour A, Jenni S, Orti-Suarez A, Schmitt J, Heitz V, Bolze F, Loureiro de Sousa P, Po C, Bonnet CS, Pallier A, Toth E, Ventura B. Four Gadolinium(III) Complexes Appended to a Porphyrin: A Water-Soluble Molecular Theranostic Agent with Remarkable Relaxivity Suited for MRI Tracking of the Photosensitizer *Inorg. Chem.* 2016; 55: 4545-54.
- [46] Ogumi K, Nakagawa T, Okada H, Sakai R, Wang H, Matsuo Y. Substituent effects in magnesium tetraethynylporphyrin with two diketopyrrolopyrrole units for bulk heterojunction organic solar cells *J. Mater. Chem. A* 2017; 5: 23067-77.

- [47] Ohta K, Tokonami S, Takahashi K, Tamura Y, Yamada H, Tominaga K. Probing Charge Carrier Dynamics in Porphyrin-Based Organic Semiconductor Thin Films by Time-Resolved THz Spectroscopy *J. Phys. Chem. B* 2017; 121: 10157-65.
- [48] Schmitt J, Heitz V, Jenni S, Sour A, Bolze F, Ventura B. π -extended porphyrin dimers as efficient near-infrared emitters and two-photon absorbers *Supramol. Chem.* 2017; 29: 769-75.
- [49] Grzybowski M, Gryko DT. Diketopyrrolopyrroles: Synthesis, Reactivity, and Optical Properties *Adv. Optical Mater.* 2015; 3: 280-320.
- [50] Kaur M, Choi DH. Diketopyrrolopyrrole: brilliant red pigment dye-based fluorescent probes and their applications *Chem. Soc. Rev.* 2015; 44: 58-77.
- [51] Wang J, Yang E, Diers JR, Niedzwiedzki DM, Kirmaier C, Bocian DF, Lindsey JS, Holten D. Distinct Photophysical and Electronic Characteristics of Strongly Coupled Dyads Containing a Perylene Accessory Pigment and a Porphyrin, Chlorin, or Bacteriochlorin *J. Phys. Chem. B* 2013; 117: 9288-304.
- [52] Yu Z, Ptaszek M. Near-IR Emissive Chlorin-Bacteriochlorin Energy-Transfer Dyads with a Common Donor and Acceptors with Tunable Emission Wavelength *J. Org. Chem.* 2013; 78: 10678-91.
- [53] Hu G, Liu R, Alexy EJ, Mandal AK, Bocian DF, Holten D, Lindsey JS. Panchromatic chromophore-tetrapyrrole light-harvesting arrays constructed from Bodipy, perylene, terrylene, porphyrin, chlorin, and bacteriochlorin building blocks *New J. Chem.* 2016; 40: 8032-52.
- [54] Mandal AK, Diers JR, Niedzwiedzki DM, Hu G, Liu R, Alexy EJ, Lindsey JS, Bocian DF, Holten D. Tailoring Panchromatic Absorption and Excited-State Dynamics of Tetrapyrrole-Chromophore (Bodipy, Rylene) Arrays-Interplay of Orbital Mixing and Configuration Interaction *J. Am. Chem. Soc.* 2017; 139: 17547-64.
- [55] Meares A, Satraitis A, Ptaszek M. BODIPY-Bacteriochlorin Energy Transfer Arrays: Toward Near-IR Emitters with Broadly Tunable, Multiple Absorption Bands *J. Org. Chem.* 2017; 82: 13068-75.
- [56] Esemoto NN, Satraitis A, Wiratan L, Ptaszek M. Symmetrical and Nonsymmetrical Meso-Meso Directly Linked Hydroporphyrin Dyads: Synthesis and Photochemical Properties *Inorg. Chem.* 2018; 57: 2977-88.
- [57] Krayer M, Ptaszek M, Kim H-J, Meneely KR, Fan D, Secor K, Lindsey JS. Expanded Scope of Synthetic Bacteriochlorins via Improved Acid Catalysis Conditions and Diverse Dihydrodipyrin-Acetals *J. Org. Chem.* 2010; 75: 1016-39.
- [58] Yu C, Liu Z, Yang Y, Yao J, Cai Z, Luo H, Zhang G, Zhang D. New dithienyl-diketopyrrolopyrrole-based conjugated molecules entailing electron withdrawing moieties for organic ambipolar semiconductors and photovoltaic materials *J. Mater. Chem. C* 2014; 2: 10101-9.
- [59] Ftouni H, Bolze F, de Rocquigny H, Nicoud J-F. Functionalized Two-Photon Absorbing Diketopyrrolopyrrole-Based Fluorophores for Living Cells Fluorescent Microscopy *Bioconjugate Chem.* 2013; 24: 942-50.
- [60] Heyer E, Lory P, Leprince J, Moreau M, Romieu A, Guardigli M, Roda A, Ziessel R. Highly fluorescent, water-soluble, bioconjugable diketopyrrolopyrrole dyes *Angew. Chem., Int. Ed.* 2015; 54: 2995-9.
- [61] Fulmer GR, Miller AJM, Sherden NH, Gottlieb HE, Nudelman A, Stoltz BM, Bercaw JE, Goldberg KI. NMR Chemical Shifts of Trace Impurities: Common Laboratory Solvents, Organics, and Gases in Deuterated Solvents Relevant to the Organometallic Chemist *Organometallics* 2010; 29: 2176-9.
- [62] Baek P, Kerr-Phillips T, Damavandi M, Chaudhary OJ, Malmstrom J, Chan EWC, Shaw P, Burn P, Barker D, Travas-Sejdic J. Highly processable, rubbery poly(n-butyl acrylate) grafted poly(phenylene vinylene)s *Eur. Polym. J.* 2016; 84: 355-65.
- [63] Yu Z, Pancholi C, Bhagavathy GV, Kang HS, Nguyen JK, Ptaszek M. Strongly Conjugated Hydroporphyrin Dyads: Extensive Modification of Hydroporphyrins' Properties by Expanding the Conjugated System *J. Org. Chem.* 2014; 79: 7919-34.
- [64] de Assis FF, Ferreira MAB, Brocksom TJ, de Oliveira KT. NIR bacteriochlorin chromophores accessed by Heck and Sonogashira cross-coupling reactions on a tetrabromobacteriochlorin derivative *Org. Biomol. Chem.* 2016; 14: 1402-12.
- [65] Meares A, Satraitis A, Akhigbe J, Santhanam N, Swaminathan S, Ehudin M, Ptaszek M. Amphiphilic BODIPY-Hydroporphyrin Energy Transfer Arrays with Broadly Tunable Absorption and Deep Red/Near-Infrared Emission in Aqueous Micelles *J. Org. Chem.* 2017; 82: 6054-70.
- [66] Meares A, Satraitis A, Santhanam N, Yu Z, Ptaszek M. Deep-Red Emissive BODIPY-Chlorin Arrays Excitable with Green and Red Wavelengths *J. Org. Chem.* 2015; 80: 3858-69.
- [67] Esemoto NN, Yu Z, Wiratan L, Satraitis A, Ptaszek M. Bacteriochlorin Dyads as Solvent Polarity Dependent Near-Infrared Fluorophores and Reactive Oxygen Species Photosensitizers *Org. Lett.* 2016; 18: 4590-3.
- [68] Bucher L, Tanguy L, Fortin D, Desbois N, Harvey PD, Sharma GD, Gros CP. An ultra-low bandgap (diketopyrrolopyrrole-porphyrin) conjugated polymer *ChemPlusChem* 2017; 82: 625-30.

- [69] Bucher L, Desbois N, Koukaras EN, Devillers CH, Biswas S, Sharma GD, Gros CP. BODIPY-diketopyrrolopyrrole-porphyrin conjugate Small Molecules for Use in Bulk Heterojunction Solar Cells *J. Mater. Chem. A* 2018; 6: 8449-61.
- [70] Yu Z, Ptaszek M. Multifunctional Bacteriochlorins from Selective Palladium-Coupling Reactions *Org. Lett.* 2012; 14: 3708-11.
- [71] Ljungdahl T, Pettersson K, Albinsson B, Maartensson J. Solvent and Base Dependence of Copper-Free Palladium-Catalyzed Cross-Couplings between Terminal Alkynes and Arylic Iodides: Development of Efficient Conditions for the Construction of Gold(III)/Free-Base Porphyrin Dimers *J. Org. Chem.* 2006; 71: 1677-87.
- [72] Wakabayashi R, Ikeda T, Kubo Y, Shinkai S, Takeuchi M. Unexpected Effects of Terminal Olefins on a Cooperative Recognition System that Implicate Olefin-Olefin Interactions *Angew. Chem., Int. Ed.* 2009; 48: 6667-70.
- [73] Brouwer AM. Standards for photoluminescence quantum yield measurements in solution *Pure Appl. Chem.* 2011; 83: 2213-28.

Near-infrared emissive bacteriochlorin-diketopyrrolopyrrole triads: Synthesis and photophysical properties

Flavien Ponsot^a, Nicolas Desbois^a, Léo Bucher^a, Mathieu Berthelot^a, Pritam Mondal^a, Claude P. Gros^{a,*}, Anthony Romieu^{a,b,*}

^aInstitut de Chimie Moléculaire de l'Université de Bourgogne, UMR 6302, CNRS, Univ. Bourgogne Franche-Comté, 9 Avenue Alain Savary, 21078 Dijon, France
Tel: +33 (0)3 80 39 61 12 or +33 (0)3 80 39 36 24
E-mail: claude.gros@u-bourgogne.fr or anthony.romieu@u-bourgogne.fr
Lab homepage: <http://www.icmub.fr>

^bInstitut Universitaire de France, 1 Rue Descartes, Bâtiment MONGE, 75231 Paris, France

Supplementary Data

Abbreviations	S5
S1 Photophysical characterizations - Experimental details	S5
S2 Analytical data	S8
Fig. S1. ¹ H NMR spectrum of compound 1 in CDCl ₃ (500 MHz).....	S8
Fig. S2. IR (ATR) spectrum of compound 3	S8
Fig. S3. ¹ H NMR spectrum of compound 3 in CDCl ₃ (500 MHz).....	S9
Fig. S4. ¹³ C NMR spectrum (JMOD) of compound 3 in CDCl ₃ (126 MHz)	S9
Fig. S5. ESI+ mass spectrum (low resolution) of compound 3	S10
Fig. S6. IR (ATR) spectrum of compound 4	S10
Fig. S7. ¹ H NMR spectrum of compound 4 in CDCl ₃ (500 MHz).....	S11
Fig. S8. ¹³ C NMR spectrum (JMOD) of compound 4 in CDCl ₃ (126 MHz)	S11
Fig. S9. ESI+ mass spectrum (low resolution) of compound 4.....	S12
Fig. S10. IR (ATR) spectrum of compound 5	S12
Fig. S11. ¹ H NMR spectrum of compound 5 in CDCl ₃ (500 MHz).....	S13
Fig. S12. ¹³ C NMR spectrum (JMOD) of compound 5 in CDCl ₃ (126 MHz)	S13
Fig. S13. ESI+ mass spectrum (low resolution) of compound 5	S14
Fig. S14. IR (ATR) spectrum of compound 6	S14
Fig. S15. ¹ H NMR spectrum of compound 6 in CDCl ₃ (500 MHz).....	S15
Fig. S16. ¹³ C NMR spectrum (JMOD) of compound 6 in CDCl ₃ (126 MHz)	S15
Fig. S17. ESI+ mass spectrum (low resolution) of compound 6.....	S16
Fig. S18. IR (ATR) spectrum of compound 7	S16
Fig. S19. ¹ H NMR spectrum of compound 7 in CDCl ₃ (500 MHz).....	S17
Fig. S20. ¹³ C NMR spectrum (JMOD) of compound 7 in CDCl ₃ (126 MHz)	S17
Fig. S21. ESI+ mass spectrum (low resolution) of compound 7.....	S18
Fig. S22. ¹ H NMR spectrum of triad BC-DPP-1 in CDCl ₃ (500 MHz)	S18
Fig. S23. MALDI-TOF mass spectrum (low resolution, positive mode) of triad BC-DPP-1	S19
Fig. S24. MALDI-TOF mass spectrum (high resolution, positive mode) of triad BC-DPP-1 1	S19
Fig. S25. ESI+ mass spectrum (low resolution) of triad BC-DPP-1	S20
Fig. S26. ¹ H NMR spectrum of triad BC-DPP-2 in CDCl ₃ (500 MHz)	S20

Fig. S27. MALDI-TOF mass spectrum (low resolution, positive mode) of triad BC-DPP-2	S21
Fig. S28. MALDI-TOF mass spectrum (high resolution, positive mode) of triad BC-DPP-2	S21
Fig. S29. ESI+ mass spectrum (low resolution) of triad BC-DPP-2	S22
Fig. S30. ¹ H NMR spectrum of triad BC-DPP-3 in CDCl ₃ (500 MHz)	S22
Fig. S31. MALDI-TOF mass spectrum (high resolution, positive mode) of triad BC-DPP-3	S23
Fig. S32. ESI+ mass spectrum (low resolution) of triad BC-DPP-3	S23
S3 Photophysical characterizations - Spectra	S24
Fig. S33. Normalized absorption, excitation (Em. 675 nm, slit 5 nm ; Ex. 300-650 nm, slit 12 nm) and emission (Ex. 550 nm, slit 5 nm ; Em. 560-725 nm, slit 5 nm) spectra of ethynyl-functionalized thienyl-DPP 1 in CHCl ₃ at 25 °C.....	S24
Fig. S34. Normalized absorption, excitation (Em. 675 nm, slit 5 nm ; Ex. 300-650 nm, slit 12 nm) and emission (Ex. 550 nm, slit 5 nm ; Em. 560-725 nm, slit 5 nm) spectra of ethynyl-functionalized thienyl-DPP 1 in toluene at 25 °C.....	S24
Fig. S35. Normalized absorption, excitation (Em. 650 nm, slit 5 nm ; Ex. 300-620 nm, slit 12 nm) and emission (Ex. 450 nm, slit 5 nm ; Em. 470-710 nm, slit 5 nm) spectra of ethynyl-functionalized phenyl-DPP 5 in CHCl ₃ at 25 °C.....	S25
Fig. S36. Normalized absorption, excitation (Em. 650 nm, slit 5 nm ; Ex. 300-620 nm, slit 12 nm) and emission (Ex. 450 nm, slit 5 nm ; Em. 470-710 nm, slit 5 nm) spectra of ethynyl-functionalized phenyl-DPP 5 in toluene at 25 °C.....	S25
Fig. S37. Normalized absorption, excitation (Em. 650 nm, slit 5 nm ; Ex. 300-620 nm, slit 12 nm) and emission (Ex. 450 nm, slit 5 nm ; Em. 470-710 nm, slit 5 nm) spectra of 3,6-diphenyl-DPP 7 in CHCl ₃ at 25 °C.....	S26
Fig. S38. Normalized absorption, excitation (Em. 650 nm, slit 5 nm ; Ex. 300-620 nm, slit 12 nm) and emission (Ex. 450 nm, slit 5 nm ; Em. 470-710 nm, slit 5 nm) spectra of 3,6-diphenyl-DPP 7 in toluene at 25 °C.....	S26
Fig. S39. Overlay of the absorbance spectra of diBr-BC, DPP 1 and BC-DPP-1 recorded in CHCl ₃ at 25 °C	S27

Fig. S40. Overlay of the emission spectra of BC-DPP-1 upon excitation at 550 nm (slit 5 nm, Em. 560-900 nm, slit 5 nm) and 720 nm (slit 5 nm, Em. 730-900 nm, slit 5 nm), recorded in CHCl ₃ at 25 °C	S27
Fig. S41. Overlay of the absorbance spectra of diBr-BC, DPP 1 and BC-DPP-1 recorded in toluene at 25 °C	S28
Fig. S42. Overlay of the emission spectra of BC-DPP-1 upon excitation at 550 nm (slit 5 nm, Em. 560-900 nm, slit 5 nm) and 720 nm (slit 5 nm, Em. 730-900 nm, slit 5 nm), recorded in toluene at 25 °C	S28
Fig. S43. Overlay of the absorbance spectra of diBr-BC, DPP 5 and BC-DPP-2 recorded in toluene at 25 °C	S29
Fig. S44. Overlay of the emission spectra of BC-DPP-2 upon excitation at 450 nm (slit 5 nm, Em. 470-900 nm, slit 5 nm) and 690 nm (slit 5 nm, Em. 700-900 nm, slit 5 nm), recorded in toluene at 25 °C	S29
Fig. S45. Overlay of the absorbance spectra of diBr-BC, DPP 7 and BC-DPP-3 recorded in toluene at 25 °C	S30
Fig. S46. Overlay of the emission spectra of BC-DPP-3 upon excitation at 450 nm (slit 5 nm, Em. 470-900 nm, slit 5 nm) and 680 nm (slit 5 nm, Em. 690-900 nm, slit 5 nm), recorded in toluene at 25 °C	S30
Fig. S47. Overlay of the absorbance and excitation (Em. 835 nm, slit 5 nm ; Ex. 300-825 nm, slit 12 nm) spectra of BC-DPP-1 recorded in CHCl ₃ at 25 °C	S31
Fig. S48. Overlay of the absorbance and excitation (Em. 835 nm, slit 5 nm ; Ex. 300-825 nm, slit 12 nm) spectra of BC-DPP-1 recorded in toluene at 25 °C	S31
Fig. S49. Overlay of the absorbance and excitation (Em. 835 nm, slit 5 nm ; Ex. 300-825 nm, slit 12 nm) spectra of BC-DPP-2 recorded in CHCl ₃ at 25 °C	S32
Fig. S50. Overlay of the absorbance and excitation (Em. 835 nm, slit 5 nm ; Ex. 300-825 nm, slit 12 nm) spectra of BC-DPP-2 recorded in toluene at 25 °C	S32
Fig. S51. Overlay of the absorbance and excitation (Em. 835 nm, slit 5 nm ; Ex. 300-825 nm, slit 12 nm) spectra of BC-DPP-3 recorded in CHCl ₃ at 25 °C	S33
Fig. S52. Overlay of the absorbance and excitation (Em. 835 nm, slit 5 nm ; Ex. 300-825 nm, slit 12 nm) spectra of BC-DPP-3 recorded in toluene at 25 °C	S33

Abbreviations

The following abbreviations are used throughout the text of the SI file: Abs., absorption; ATR, attenuated total reflectance; BC, bacteriochlorin; DMSO, dimethylsulfoxide; DPP, diketopyrrolopyrrole; Em., emission; EtOH, ethanol; ESI, electrospray ionisation; Ex., excitation; ICG, indocyanine green; IR, infrared; JMOD, J modulation pulse sequence; NMR, nuclear magnetic resonance; SR101, sulforhodamine 101.

S1 Photophysical characterizations - Experimental details

Fluorescein disodium salt hydrate was provided by Alfa Aesar (#A11659). SR101 (free acid, 99%) and ICG (IR-125, pure, laser grade) were purchased from Acros (#419945000 and #412541000). DMSO (+99.9% for spectroscopy was provided by Acros. CHCl₃ (RPE - ISO - for analysis, stabilized with EtOH), EtOH (absolute anhydrous RE) and toluene (HPLC grade) were purchased from Carlo Erba (for the first two mentioned) and Biosolve respectively.

Stock solutions (1.0 mg/mL) of DPP derivatives were prepared either in CHCl₃ (DPP dye **1**) or in DMSO (DPP dyes **5** and **7**) and subsequently diluted with the corresponding solvent for UV-vis absorption and fluorescence measurements.

Stock solutions (1.0 mg/mL) of triad BC-DPP were prepared in CHCl₃ and subsequently diluted with the corresponding solvent for UV-vis absorption and fluorescence measurements.

Emission spectra were recorded with the following parameters (shutter: Auto Open):

- DPP dye **1**, Ex. 550 nm, slit 5 nm ; Em. 560-725 nm, slit 5 nm,
- DPP dye **5**, Ex. 450 nm, slit 5 nm ; Em. 470-710 nm, slit 5 nm,
- DPP dye **7**, Ex. 450 nm, slit 5 nm ; Em. 470-710 nm, slit 5 nm,
- **BC-DPP-1**, excitation Q_y band, Ex. 720 nm, slit 5 nm, Em. 730-900 nm, slit 5 nm,
- **BC-DPP-2**, excitation Q_y band, Ex. 690 nm, slit 5 nm ; Em. 700-900 nm, slit 5 nm,
- **BC-DPP-3**, excitation Q_y band, Ex. 680 nm, slit 5 nm ; Em. 690-900 nm, slit 5 nm.
- **BC-DPP-1**, excitation DPP, Ex. 550 nm, slit 5 nm, Em. 560-900 nm, slit 5 nm,
- **BC-DPP-2**, excitation DPP, Ex. 450 nm, slit 5 nm ; Em. 470-900 nm, slit 5 nm,
- **BC-DPP-3**, excitation DPP, Ex. 450 nm, slit 5 nm ; Em. 470-900 nm, slit 5 nm.

Excitation spectra were recorded with the following parameters (shutter: Auto Open):

- DPP dye **1**, Em. 675 nm, slit 5 nm ; Ex. 300-650 nm, slit 12 nm,
- DPP dye **5**, Em. 650 nm, slit 5 nm ; Ex. 300-630 nm, slit 12 nm,
- DPP dye **7**, Em. 650 nm, slit 5 nm ; Ex. 300-630 nm, slit 12 nm,
- **BC-DPP-1**, Em. 835 nm, slit 5 nm, Ex. 300-825 nm, slit 12 nm,
- **BC-DPP-2**, Em. 835 nm, slit 5 nm, Ex. 300-825 nm, slit 12 nm,
- **BC-DPP-3**, Em. 835 nm, slit 5 nm, Ex. 300-825 nm, slit 12 nm.

All fluorescence spectra were corrected until 850 nm.

Fluorescence quantum yields were measured at 25 °C by a relative method using the suitable standard (see Table S1, dilution by a factor of 30 between absorption and fluorescence measurements except those performed in the NIR range for ICG and triads, no dilution). The following equation was used to determine the relative fluorescence quantum yield:

$$\Phi_F(x) = (A_s/A_x)(F_x/F_s)(n_x/n_s)^2\Phi_F(s)$$

where A is the absorbance (in the range of 0.01-0.1 A.U.), F is the area under the emission curve, n is the refractive index of the solvents (at 25 °C) used in measurements, and the subscripts s and x represent standard and unknown, respectively.

Table S1. Experimental conditions used for the determination of fluorescence quantum yields.

Fluorophore	Solvent ^a	λ Ex (nm)	Standard (std) ^b	$\Phi_{F(\text{std})} / \text{solvent}^b$	Φ_F
1	CHCl ₃	550	SR101	0.95 / EtOH	0.55
1	toluene	550	SR101	0.95 / EtOH	0.77
5	CHCl ₃	450	Fluorescein	0.90 / 0.1 M NaOH	1.00
5	toluene	450	Fluorescein	0.90 / 0.1 M NaOH	0.95
7	CHCl ₃	450	Fluorescein	0.90 / 0.1 M NaOH	0.89
7	toluene	450	Fluorescein	0.90 / 0.1 M NaOH	0.88
BC-DPP-1	CHCl ₃	720	ICG	0.106 / DMSO	0.075
BC-DPP-1	toluene	720	ICG	0.106 / DMSO	0.08
BC-DPP-2	CHCl ₃	690	ICG	0.106 / DMSO	0.11
BC-DPP-2	toluene	690	ICG	0.106 / DMSO	0.12
BC-DPP-3	CHCl ₃	680	ICG	0.106 / DMSO	0.065

BC-DPP-3	toluene	680	ICG	0.106 / DMSO	0.13
-----------------	---------	-----	-----	-----------------	------

^a The following refractive index values were used: 1.446 for CHCl₃, 1.479 for DMSO, 1.361 for EtOH, 1.497 for toluene and 1.337 for 0.1 M aq. NaOH.

^b Brouwer AM. Standards for photoluminescence quantum yield measurements in solution Pure Appl. Chem. 2011; 83: 2213-28.

Energy transfer efficiency was calculated based on the equation $\{100 \times [1 - (\Phi_F \text{ donor in triad})/(\Phi_F \text{ free donor})]\}$.

The following DPP dyes were used as free donors and their fluorescence quantum yields within the triads were determined as previously described:

1 for **BC-DPP-1** (Ex. at 550 nm, Em. 560-725 nm, slit 5 nm), Φ_F (**1** in **BC-DPP-1**) = 0.013 in CHCl₃ and 0.02 in toluene,

5 for **BC-DPP-2** (Ex. at 450 nm, Em. 470-710 nm, slit 5 nm), Φ_F (**5** in **BC-DPP-2**) = 0.013 in CHCl₃ and 0.013 in toluene,

7 for **BC-DPP-3** (Ex. 450 nm, Em. 470-710 nm), Φ_F (**7** in **BC-DPP-3**) = 0.04 in CHCl₃ and 0.036 in toluene,

S2 Analytical data

Fig. S1. ^1H NMR spectrum of compound 1 in CDCl_3 (500 MHz)

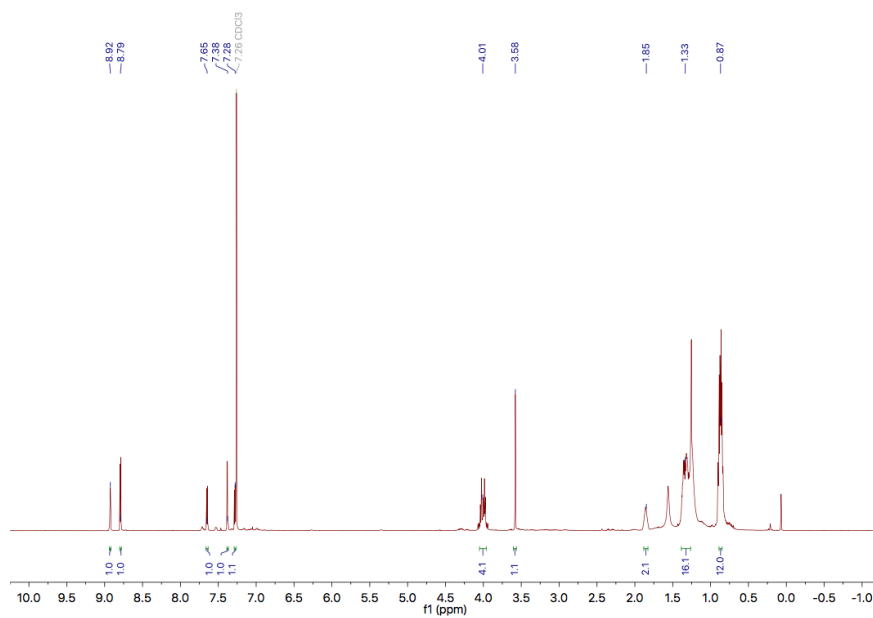
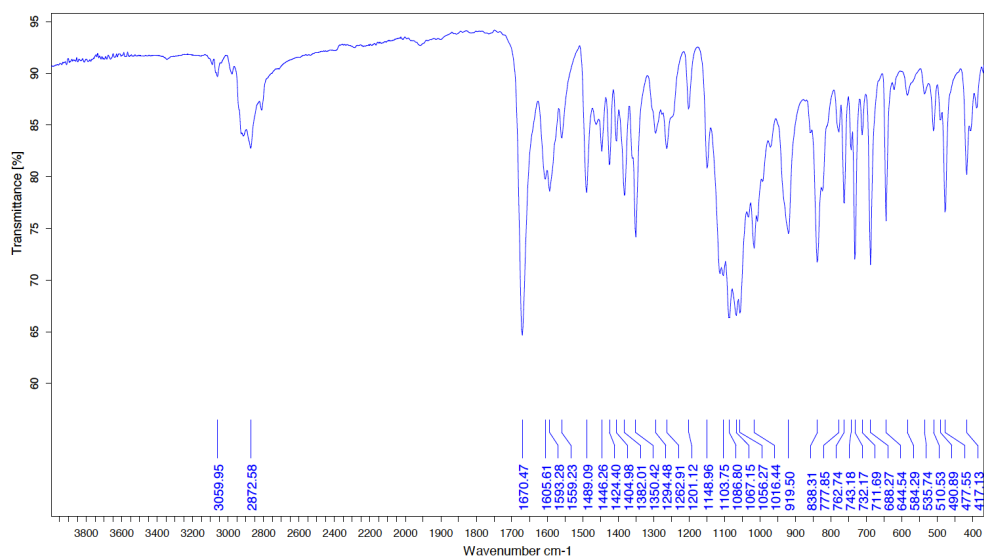


Fig. S2. IR (ATR) spectrum of compound 3



Echantillon :	Spectre :
18LKG004	U[(18O)2(NMA)2(H2O).6 (dans D:\rdata_VERTEX\brande
	Technique : MIR ATR A225 Diamant 7000 - 370 cm-1
	Opérateur : quesneau
résolution : 4 cm-1 (32 scans)	mesuré le 01/02/2018 sur VERTEX 70V

Fig. S3. ^1H NMR spectrum of compound 3 in CDCl_3 (500 MHz)

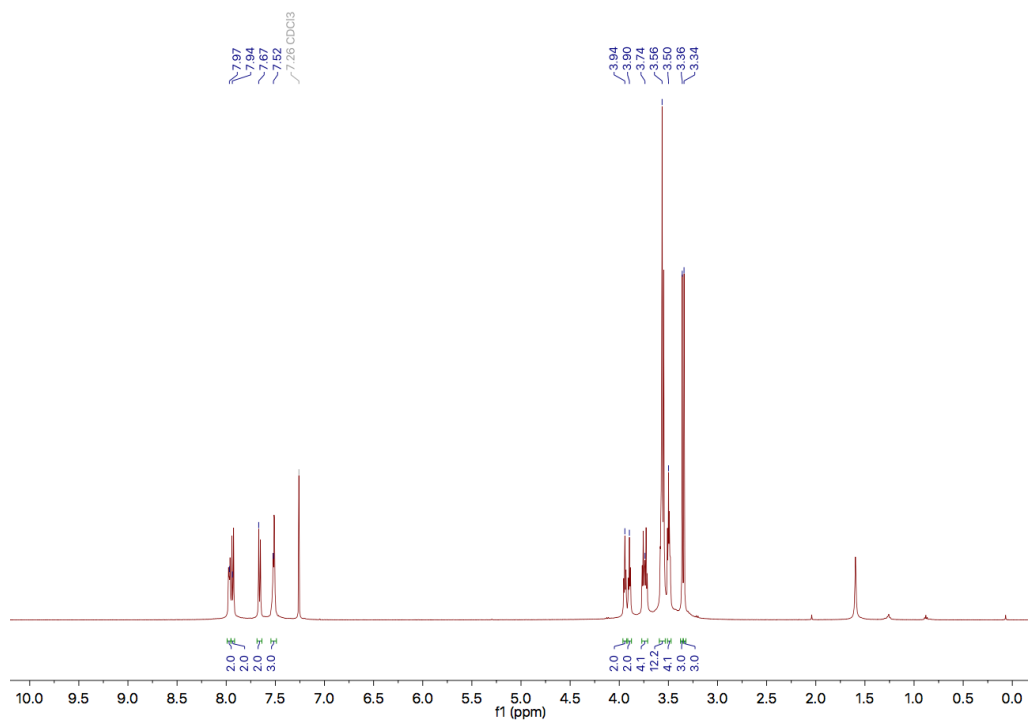


Fig. S4. ^{13}C NMR spectrum (JMOD) of compound 3 in CDCl_3 (126 MHz)

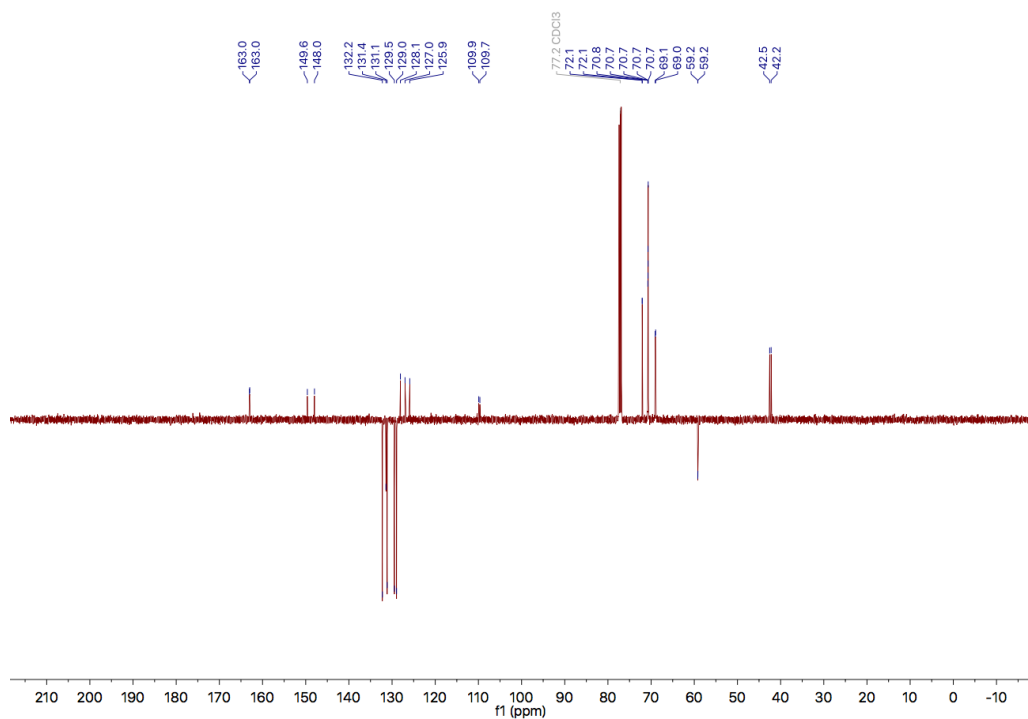


Fig. S5. ESI+ mass spectrum (low resolution) of compound 3

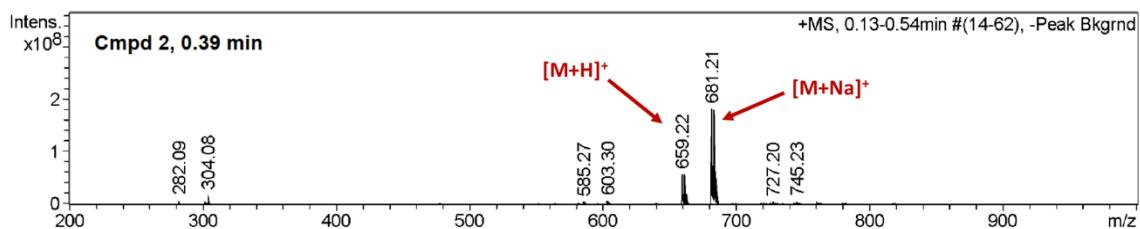


Fig. S6. IR (ATR) spectrum of compound 4

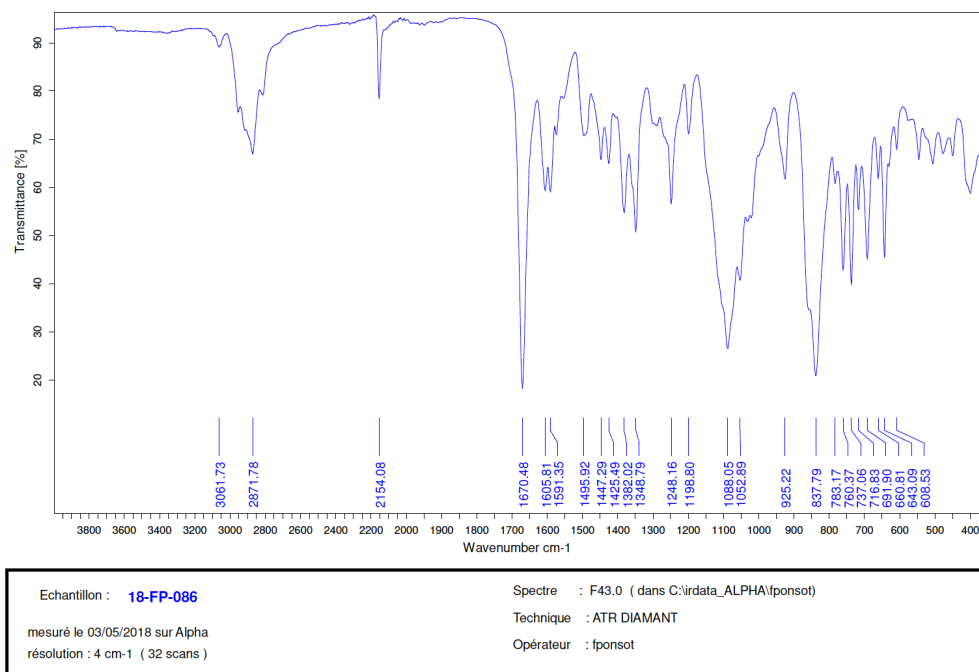


Fig. S7. ^1H NMR spectrum of compound 4 in CDCl_3 (500 MHz)

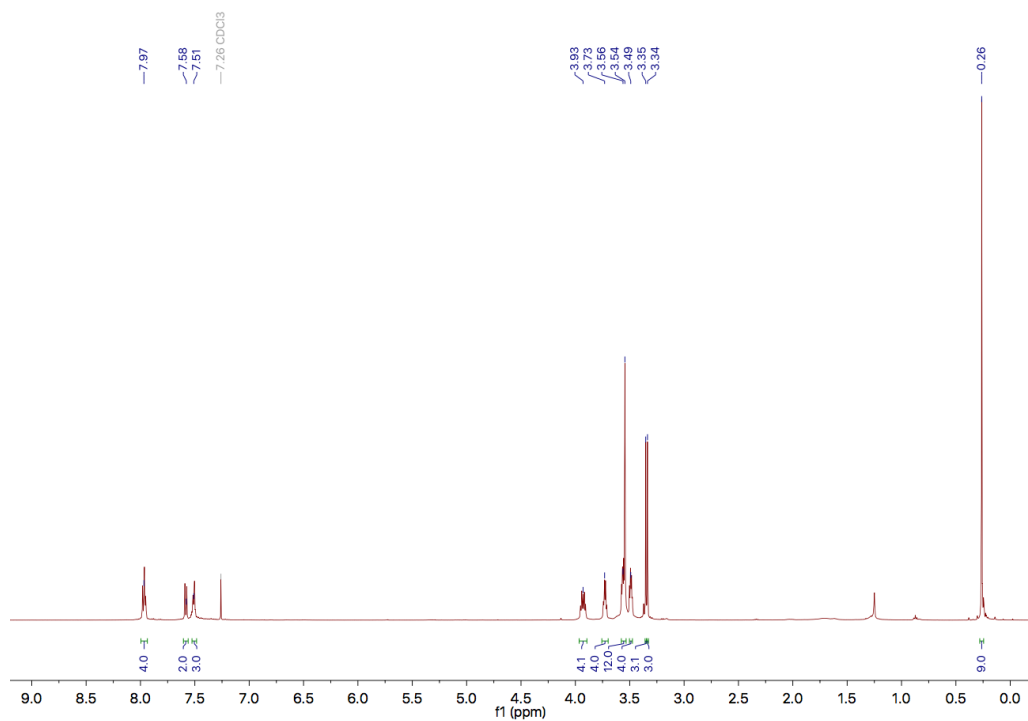


Fig. S8. ^{13}C NMR spectrum (JMOD) of compound 4 in CDCl_3 (126 MHz)

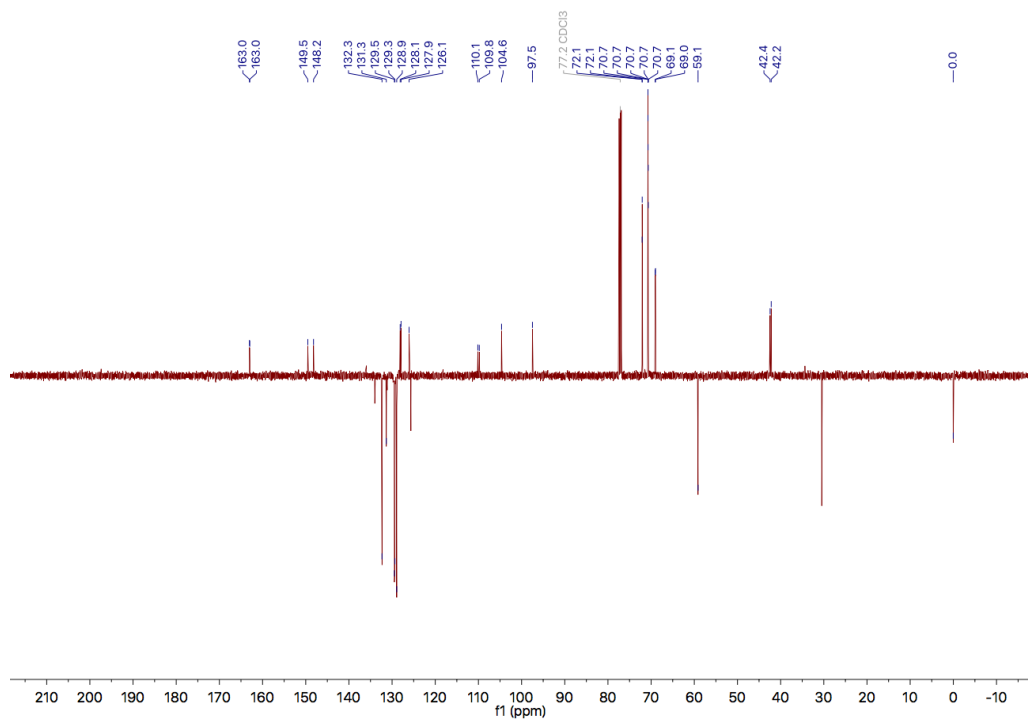


Fig. S9. ESI+ mass spectrum (low resolution) of compound 4

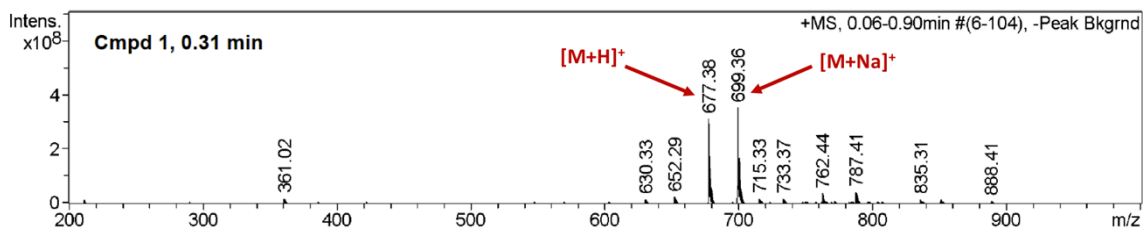
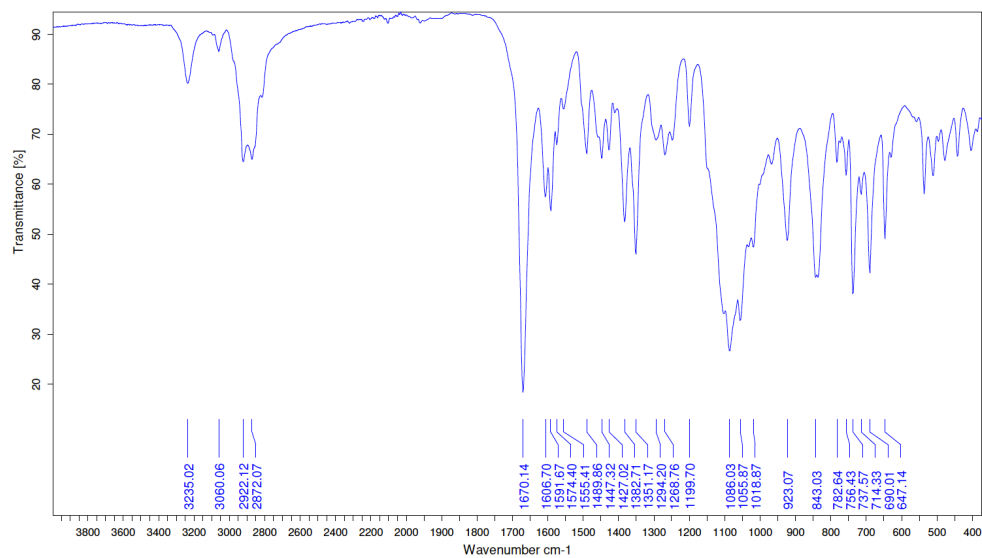


Fig. S10. IR (ATR) spectrum of compound 5



Echantillon : 18-FP-118	Spectre : F43.1 (dans C:\irdata_ALPHA\fpnsot)
mesuré le 03/05/2018 sur Alpha	Technique : ATR DIAMANT
résolution : 4 cm-1 (32 scans)	Opérateur : fponsot

Fig. S11. ^1H NMR spectrum of compound 5 in CDCl_3 (500 MHz)

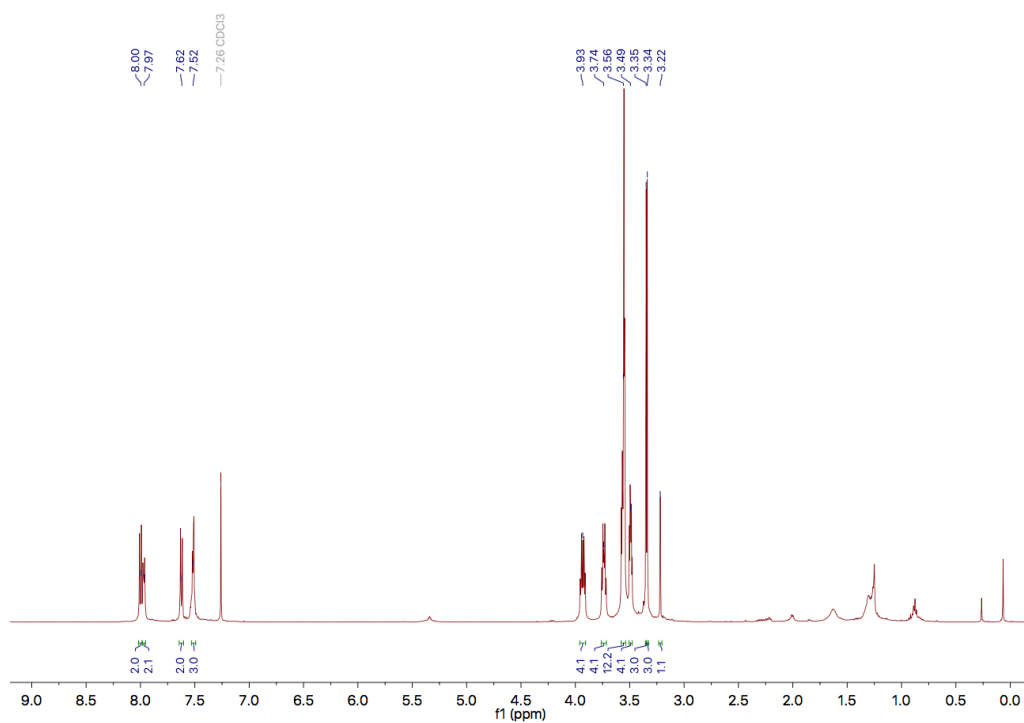


Fig. S12. ^{13}C NMR spectrum (JMOD) of compound 5 in CDCl_3 (126 MHz)

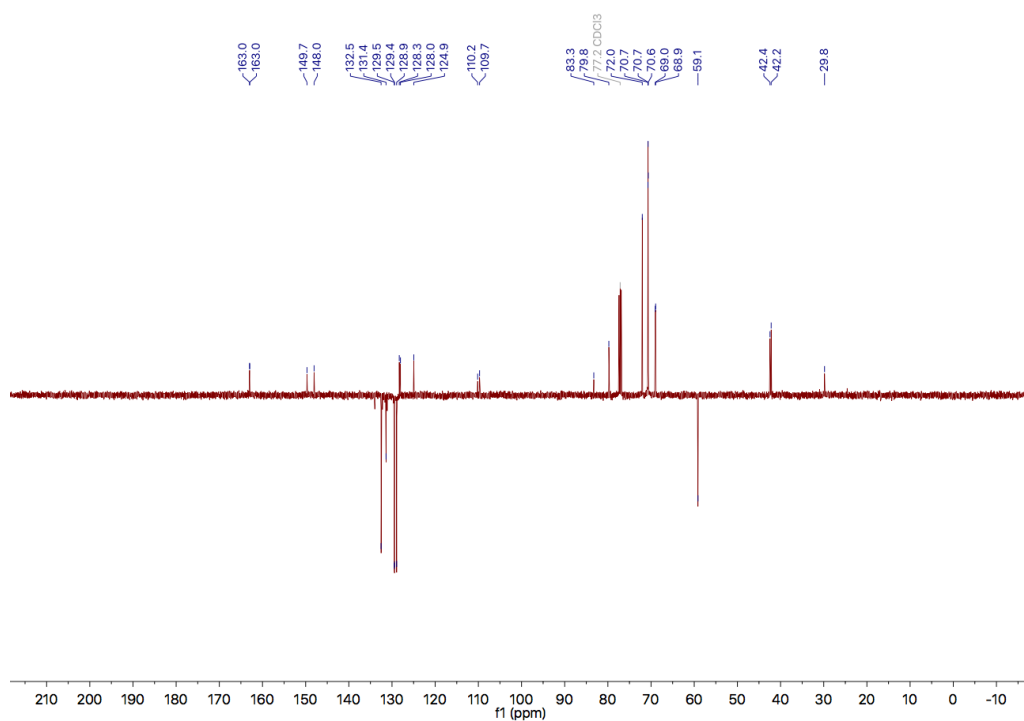


Fig. S13. ESI+ mass spectrum (low resolution) of compound 5

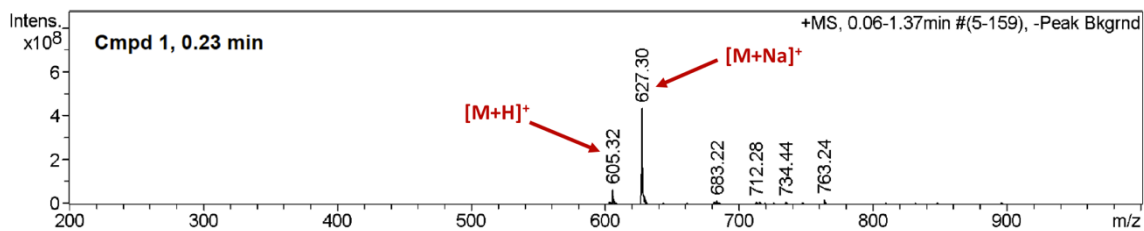
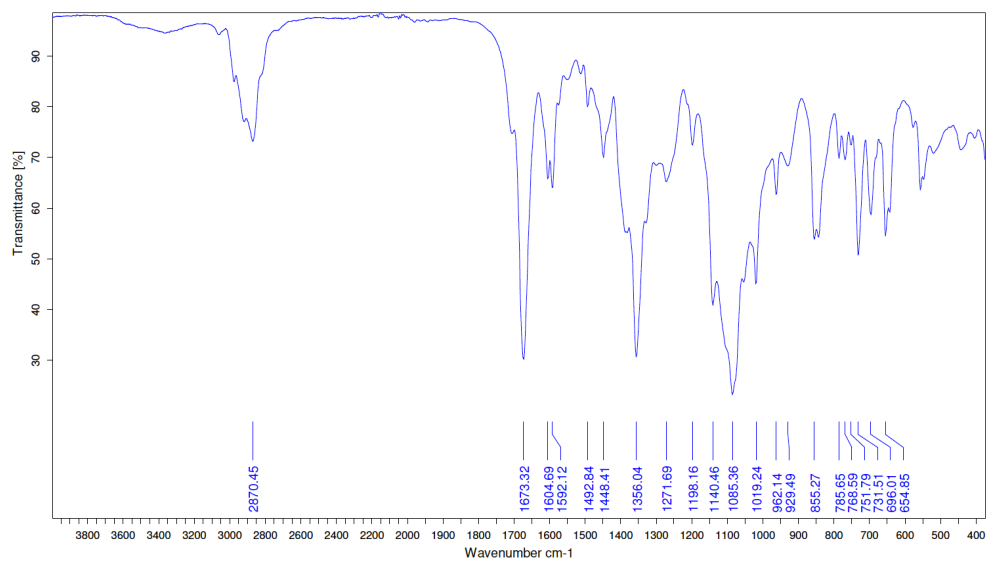


Fig. S14. IR (ATR) spectrum of compound 6



Echantillon : **18-FP-115** Spectre : F43.2 (dans C:\virdata_ALPHA\fpnsot)
mesuré le 03/05/2018 sur Alpha Technique : ATR DIAMANT
résolution : 4 cm⁻¹ (32 scans) Opérateur : fpnsot

Fig. S15. ^1H NMR spectrum of compound 6 in CDCl_3 (500 MHz)

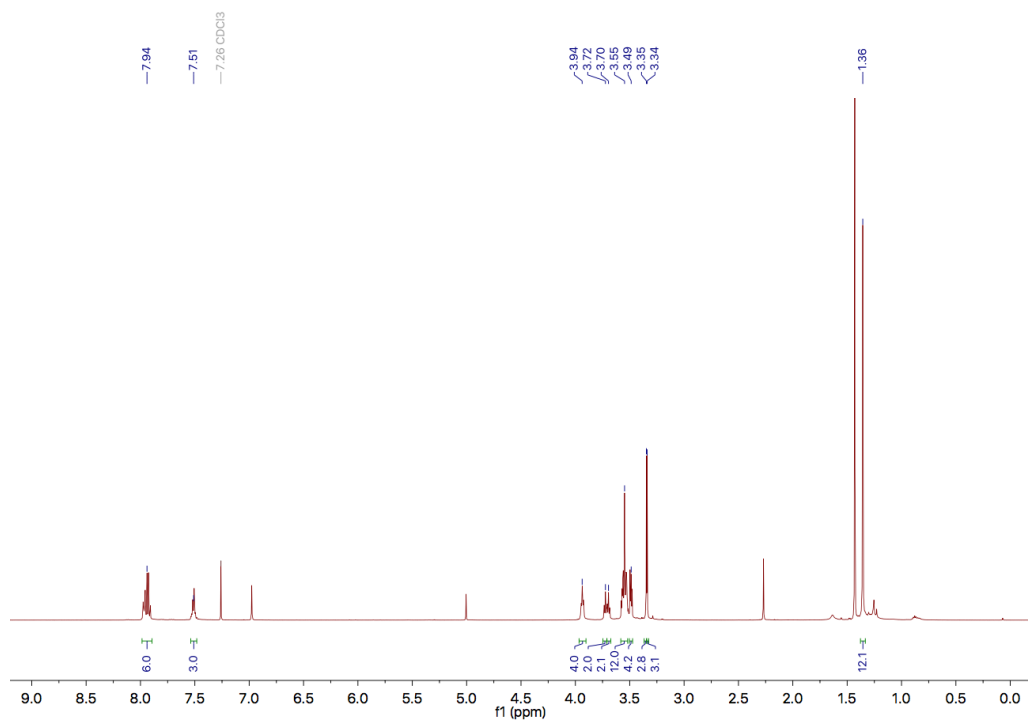


Fig. S16. ^{13}C NMR spectrum (JMOD) of compound 6 in CDCl_3 (126 MHz)

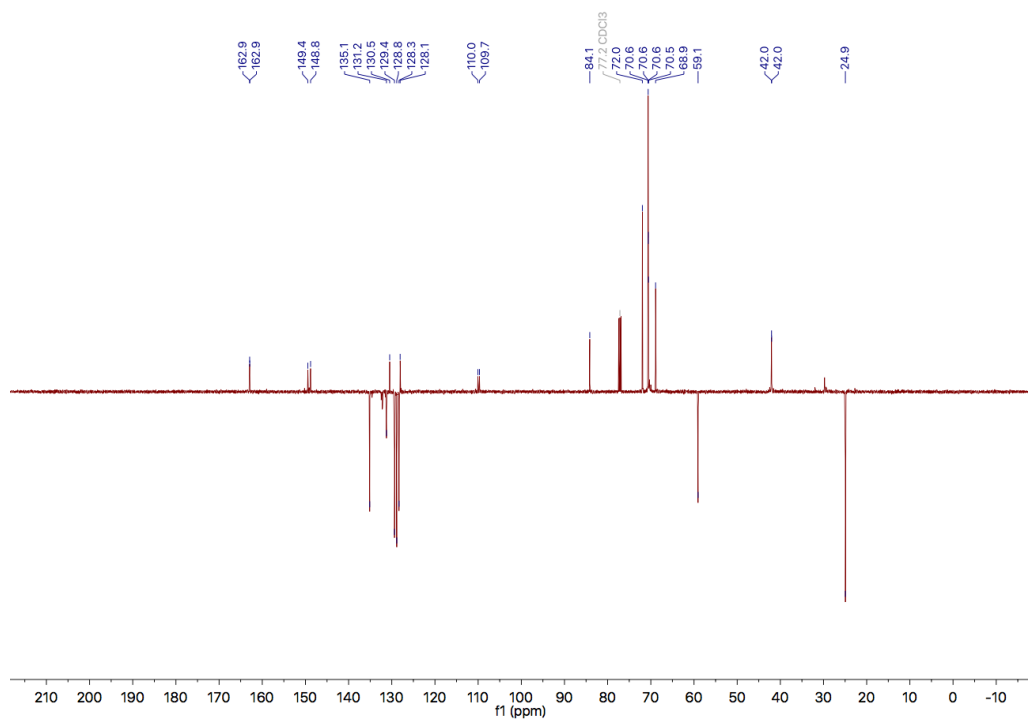


Fig. S17. ESI+ mass spectrum (low resolution) of compound 6

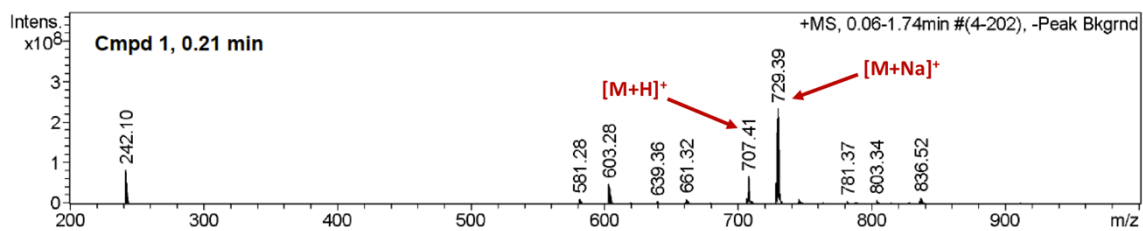
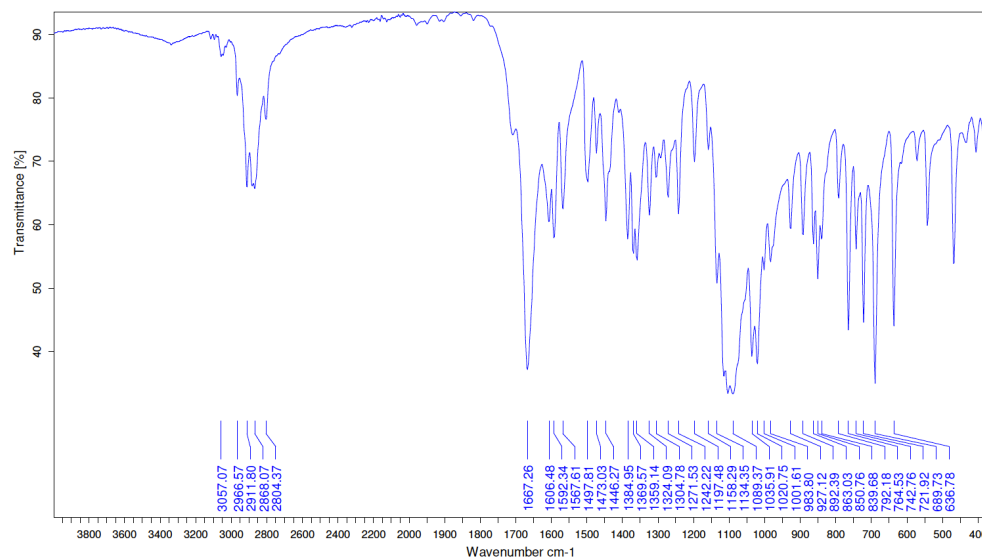


Fig. S18. IR (ATR) spectrum of compound 7



Echantillon : 18-FP-116

Spectre : F43.3 (dans C:\irdata_ALPHA\lponso)

mesuré le 03/05/2018 sur Alpha
résolution : 4 cm^{-1} (32 scans)

Technique : ATR DIAMANT
Opérateur : lponso

Fig. S19. ^1H NMR spectrum of compound 7 in CDCl_3 (500 MHz)

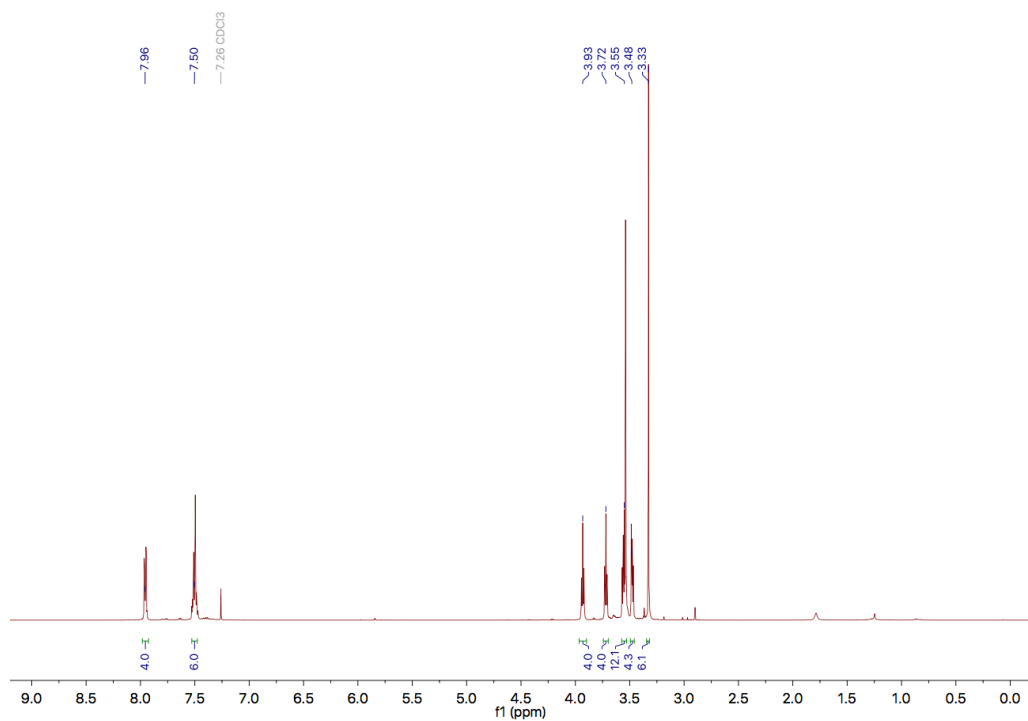


Fig. S20. ^{13}C NMR spectrum (JMOD) of compound 7 in CDCl_3 (126 MHz)

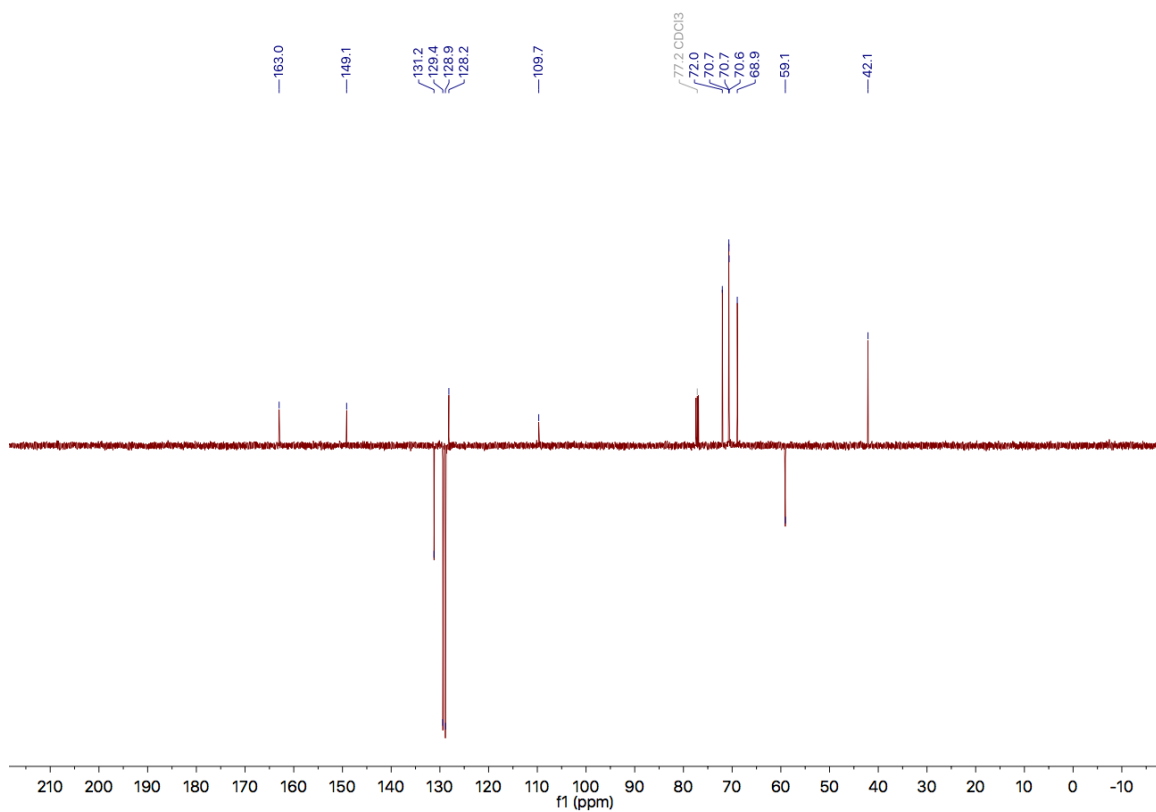


Fig. S21. ESI+ mass spectrum (low resolution) of compound 7

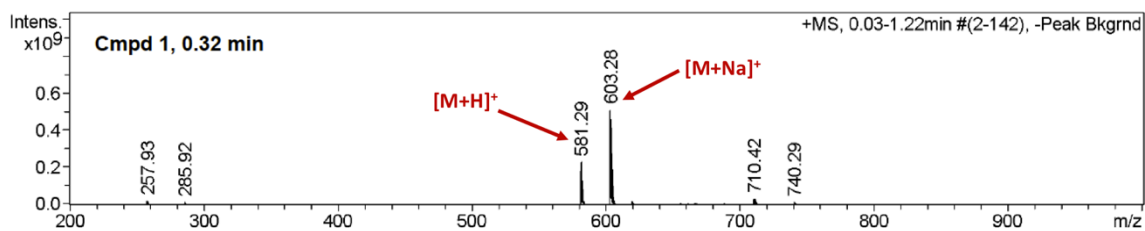


Fig. S22. ¹H NMR spectrum of triad BC-DPP-1 in CDCl₃ (500 MHz)

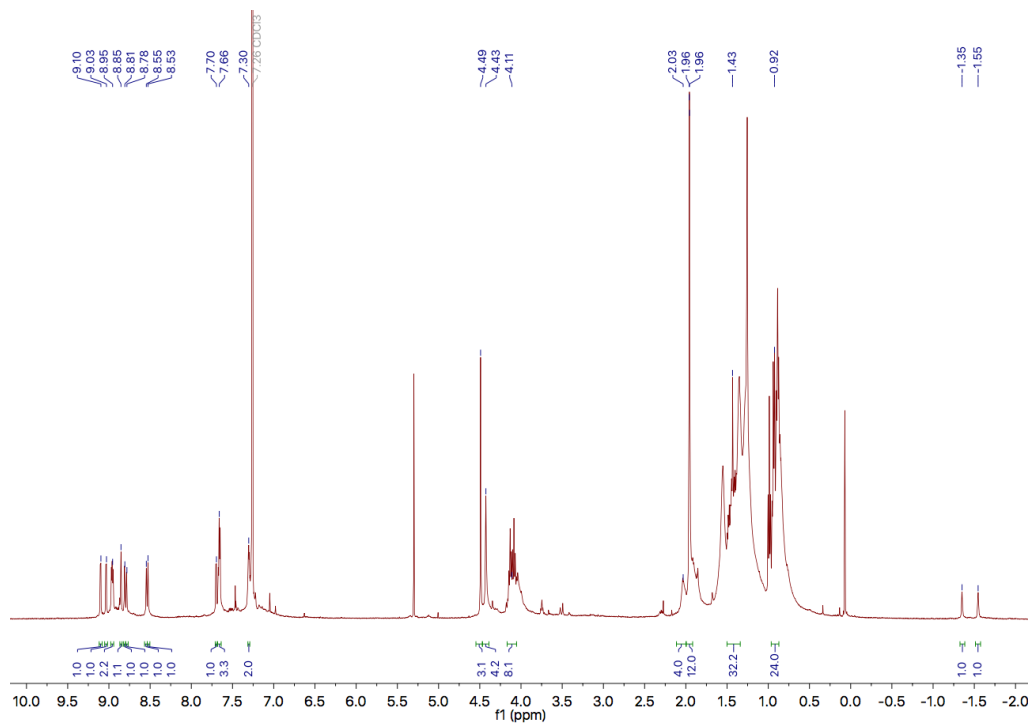


Fig. S23. MALDI-TOF mass spectrum (low resolution, positive mode) of triad BC-DPP-1

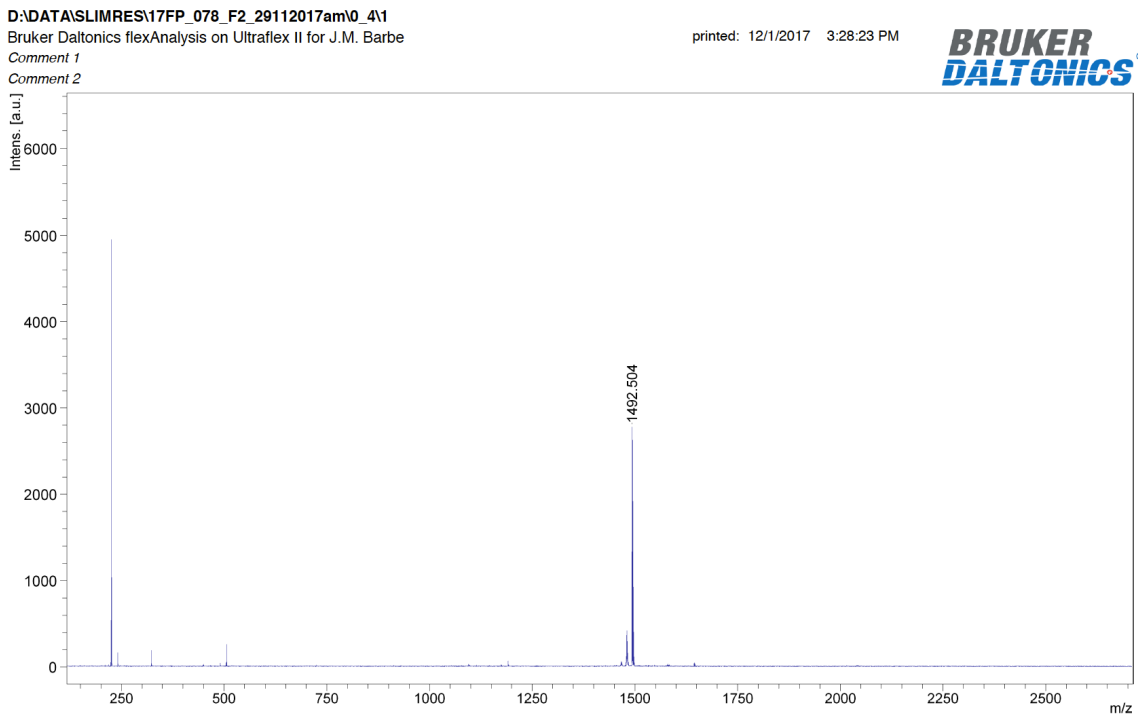


Fig. S24. MALDI-TOF mass spectrum (high resolution, positive mode) of triad BC-DPP-1

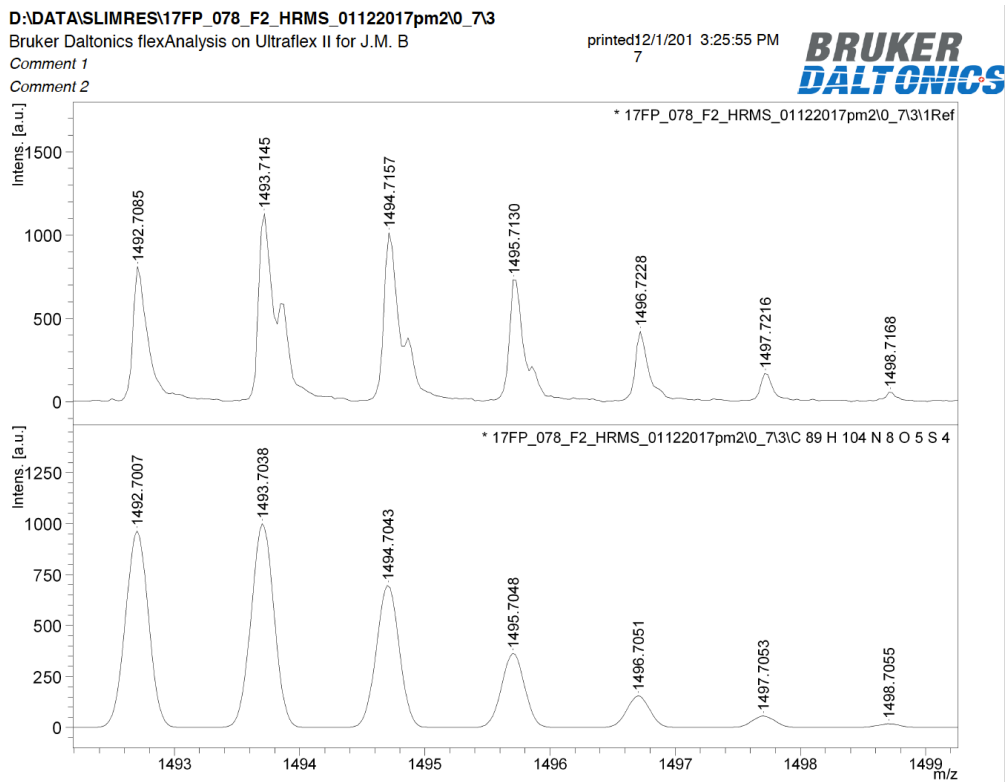


Fig. S25. ESI+ mass spectrum (low resolution) of triad BC-DPP-1

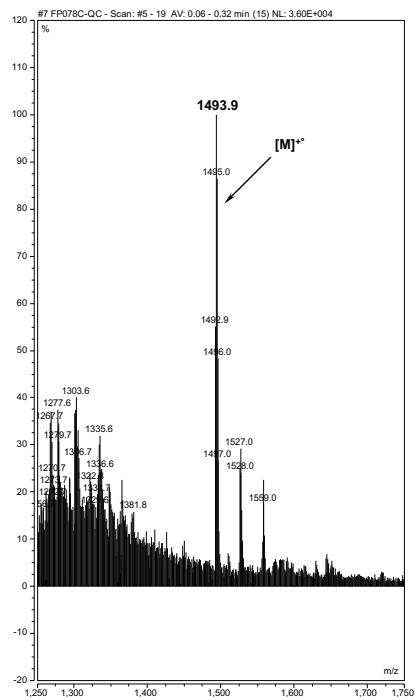


Fig. S26. ^1H NMR spectrum of triad BC-DPP-2 in CDCl_3 (500 MHz)

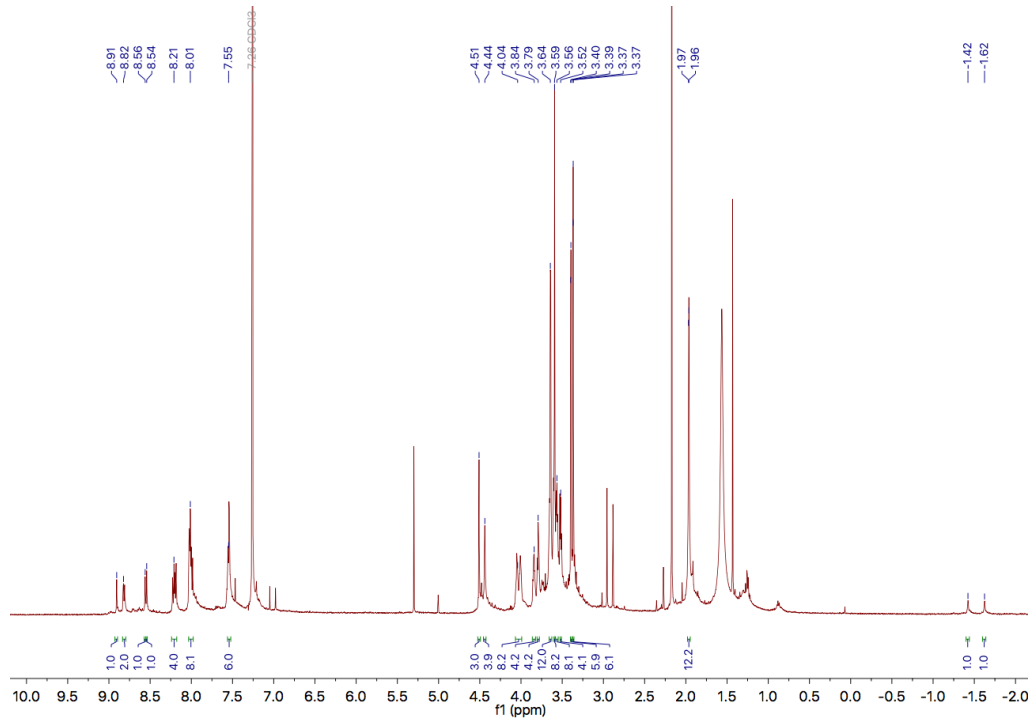


Fig. S27. MALDI-TOF mass spectrum (low resolution, positive mode) of triad BC-DPP-2

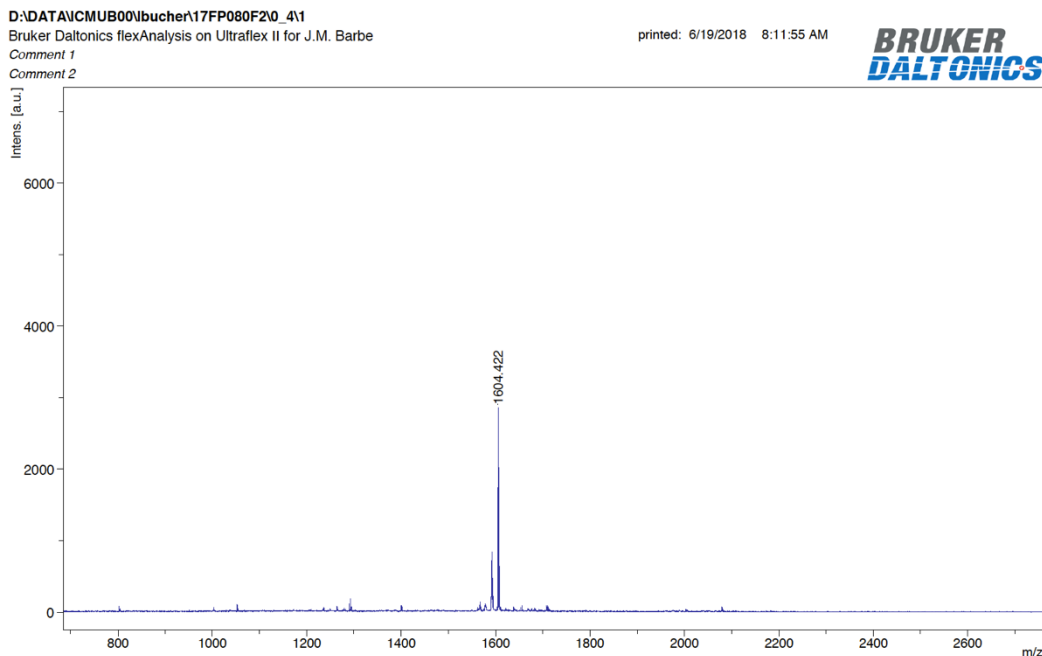


Fig. S28. MALDI-TOF mass spectrum (high resolution, positive mode) of triad BC-DPP-2

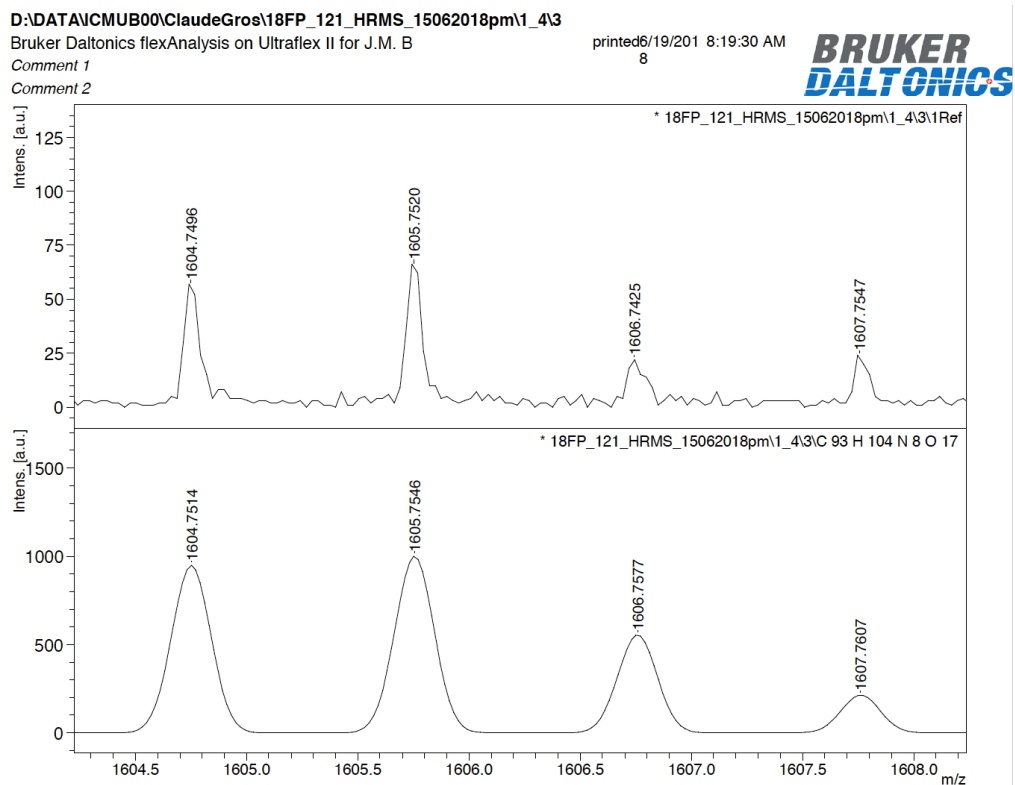


Fig. S29. ESI+ mass spectrum (low resolution) of triad BC-DPP-2

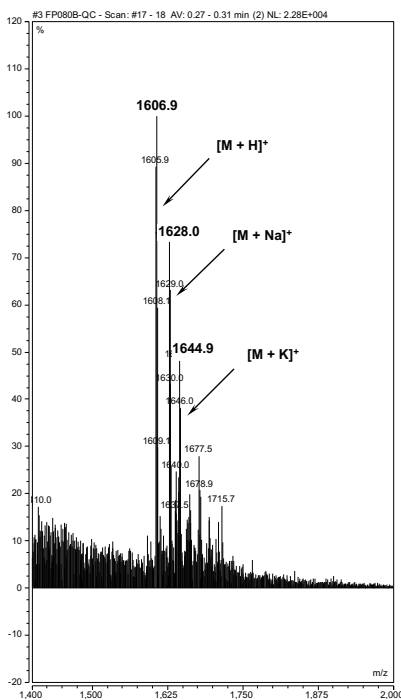


Fig. S30. ¹H NMR spectrum of triad BC-DPP-3 in CDCl₃ (500 MHz)

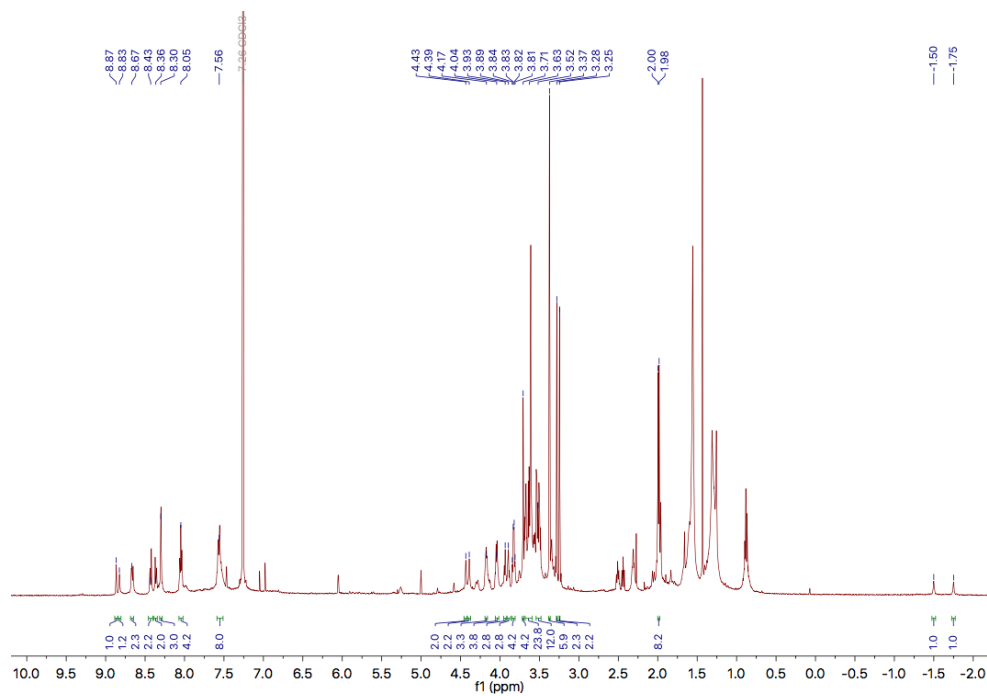


Fig. S31. MALDI-TOF mass spectrum (high resolution, positive mode) of triad BC-DPP-3

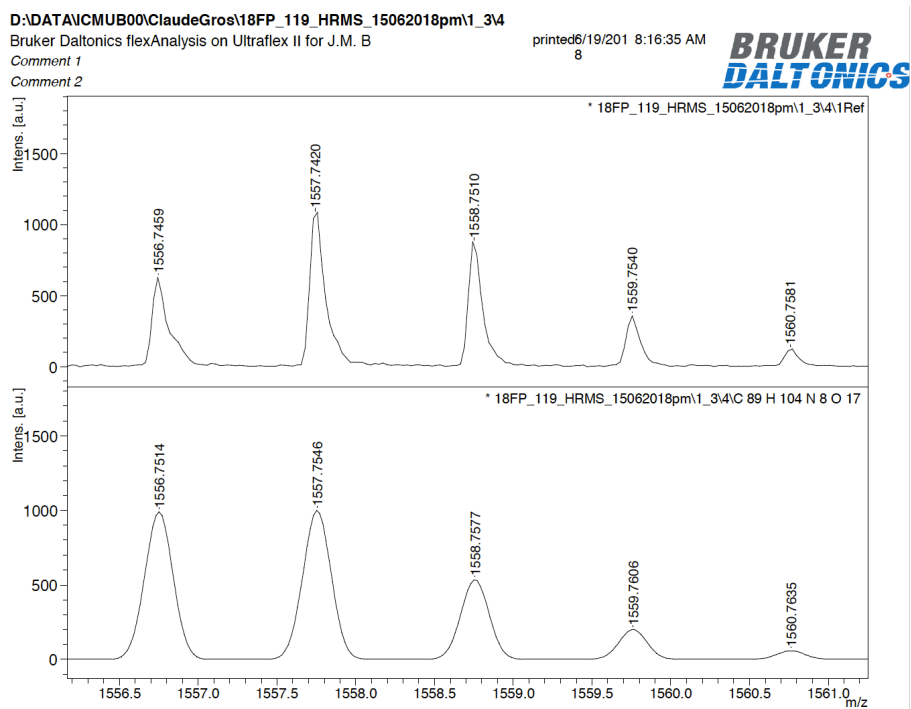
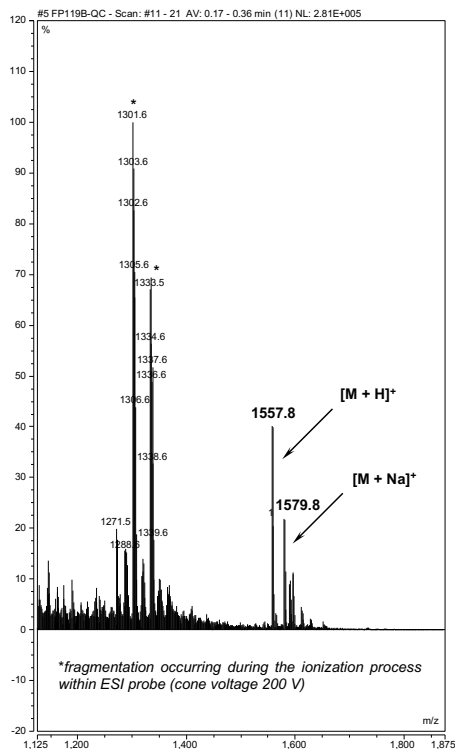


Fig. S32. ESI+ mass spectrum (low resolution) of triad BC-DPP-3



S3 Photophysical characterizations - Spectra

Please note: For some excitation spectra, peak at 325/337 nm ($\lambda_{ex}/2$) assigned to Rayleigh scattering is observed. Emission spectra cannot be corrected in the range 850-900 nm, which explains the artifact observed at 850 nm (this also the case with standard namely ICG).

Fig. S33. Normalized absorption, excitation (Em. 675 nm, slit 5 nm ; Ex. 300-650 nm, slit 12 nm) and emission (Ex. 550 nm, slit 5 nm ; Em. 560-725 nm, slit 5 nm) spectra of ethynyl-functionalized thienyl-DPP 1 in CHCl_3 at 25 °C

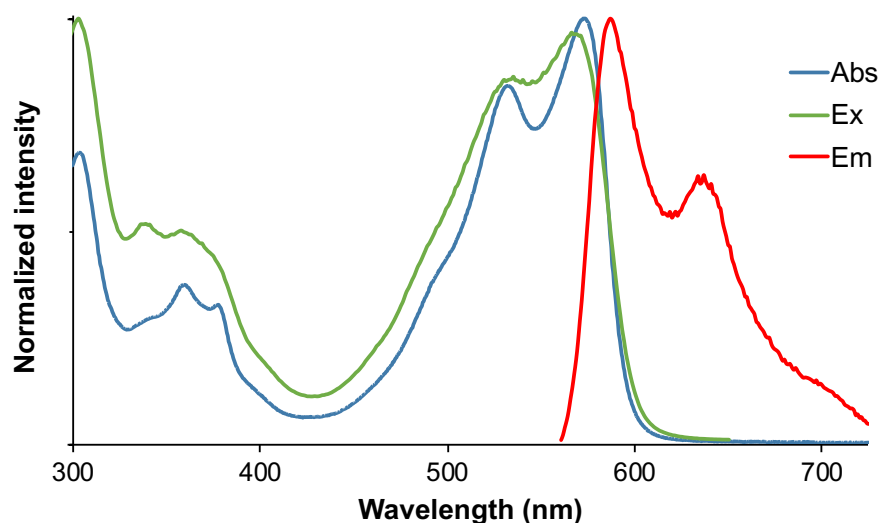


Fig. S34. Normalized absorption, excitation (Em. 675 nm, slit 5 nm ; Ex. 300-650 nm, slit 12 nm) and emission (Ex. 550 nm, slit 5 nm ; Em. 560-725 nm, slit 5 nm) spectra of ethynyl-functionalized thienyl-DPP 1 in toluene at 25 °C

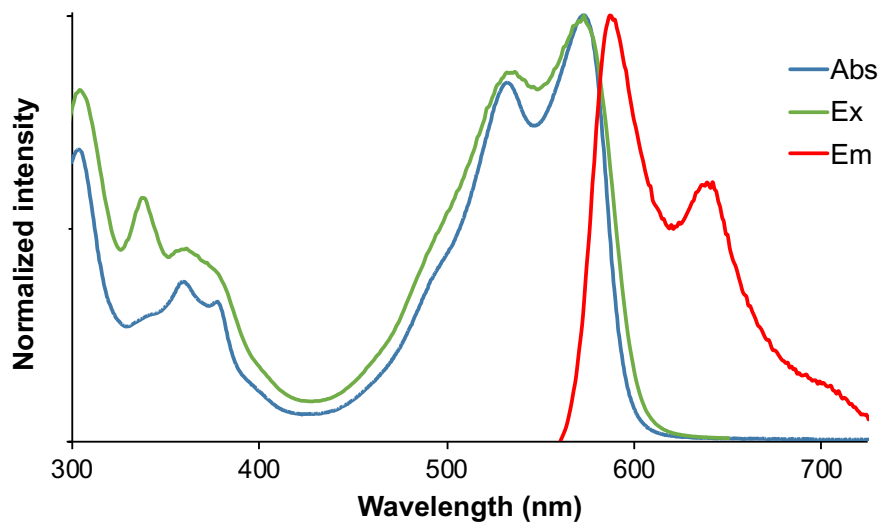


Fig. S35. Normalized absorption, excitation (Em. 650 nm, slit 5 nm ; Ex. 300-620 nm, slit 12 nm) and emission (Ex. 450 nm, slit 5 nm ; Em. 470-710 nm, slit 5 nm) spectra of ethynyl-functionalized phenyl-DPP 5 in CHCl₃ at 25 °C

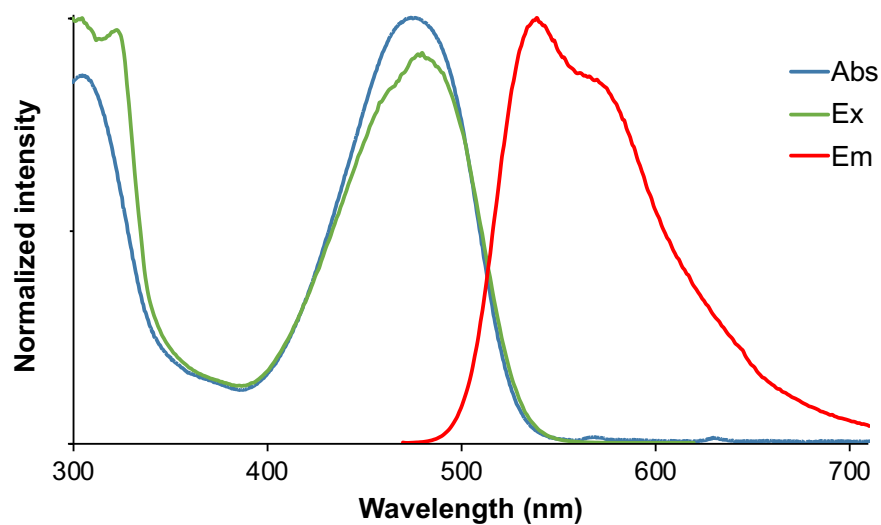


Fig. S36. Normalized absorption, excitation (Em. 650 nm, slit 5 nm ; Ex. 300-620 nm, slit 12 nm) and emission (Ex. 450 nm, slit 5 nm ; Em. 470-710 nm, slit 5 nm) spectra of ethynyl-functionalized phenyl-DPP 5 in toluene at 25 °C

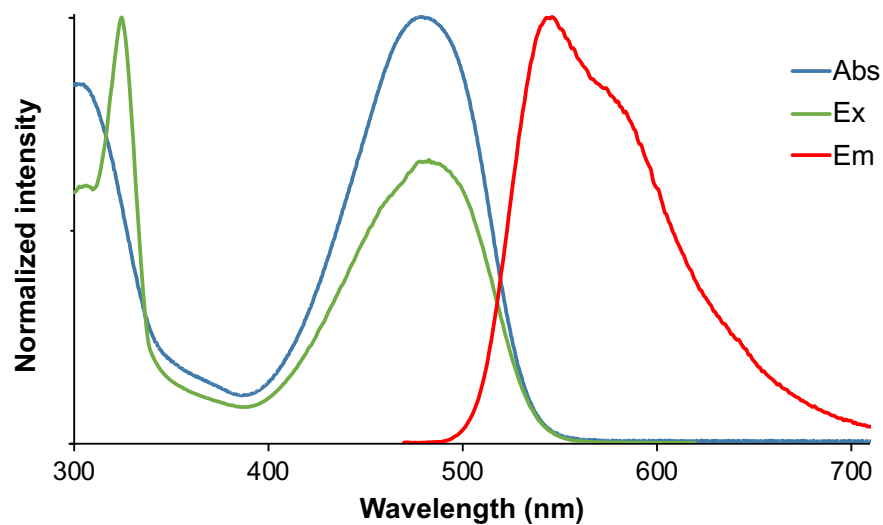


Fig. S37. Normalized absorption, excitation (Em. 650 nm, slit 5 nm ; Ex. 300-620 nm, slit 12 nm) and emission (Ex. 450 nm, slit 5 nm ; Em. 470-710 nm, slit 5 nm) spectra of 3,6-diphenyl-DPP 7 in CHCl_3 at 25 °C

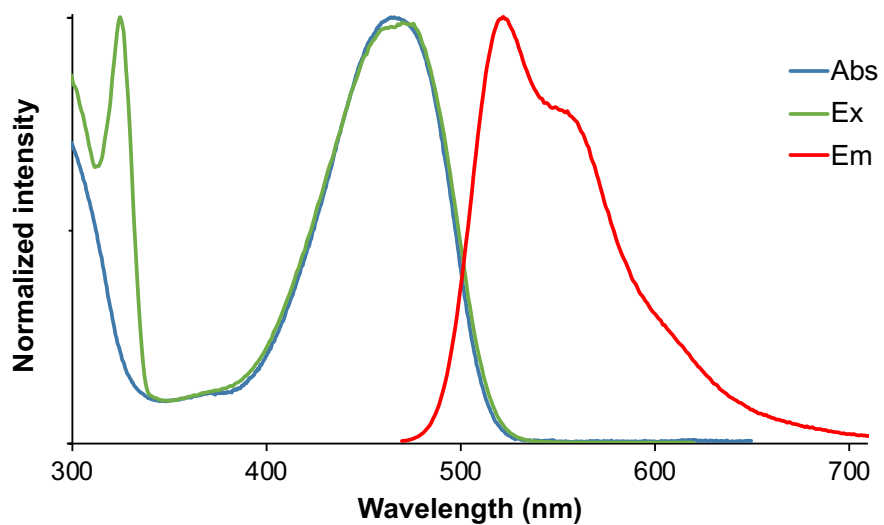


Fig. S38. Normalized absorption, excitation (Em. 650 nm, slit 5 nm ; Ex. 300-620 nm, slit 12 nm) and emission (Ex. 450 nm, slit 5 nm ; Em. 470-710 nm, slit 5 nm) spectra of 3,6-diphenyl-DPP 7 in toluene at 25 °C

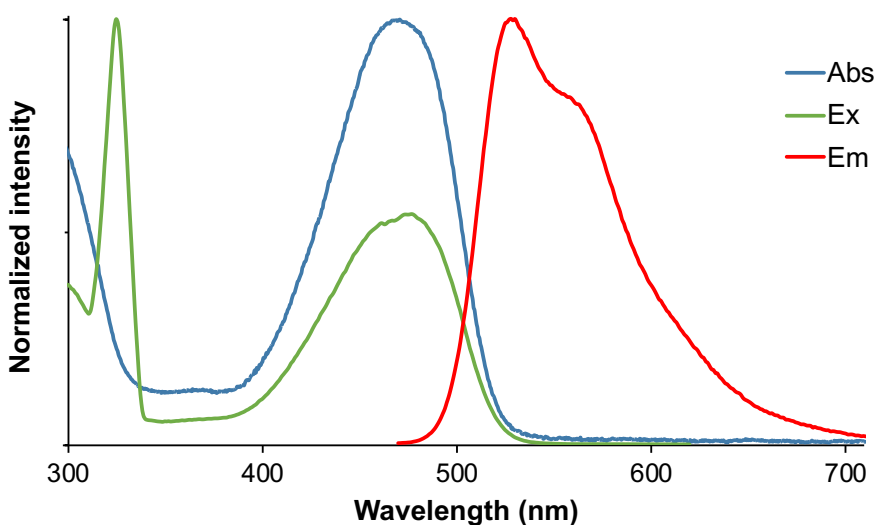


Fig. S39. Overlay of the absorbance spectra of diBr-BC, DPP 1 and BC-DPP-1 recorded in CHCl₃ at 25 °C

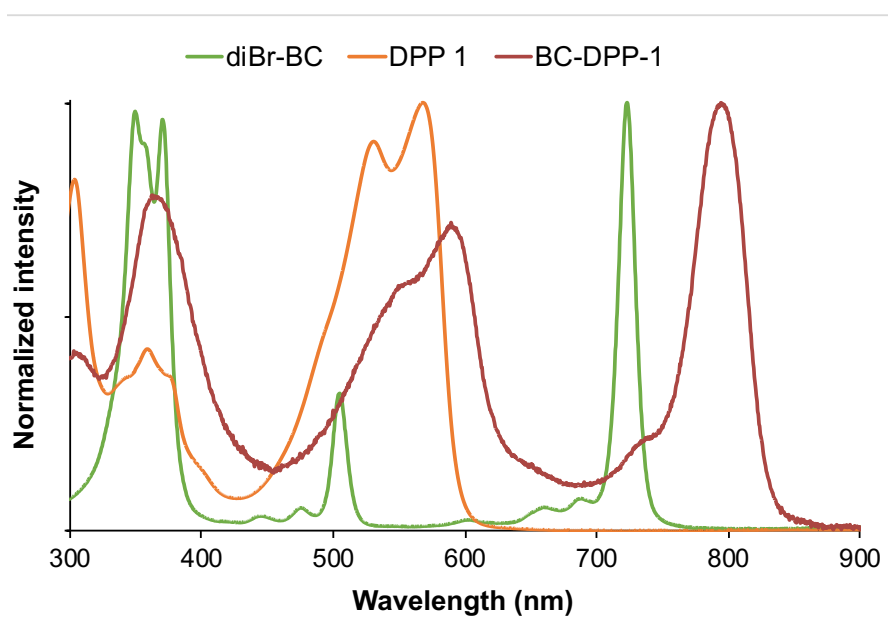


Fig. S40. Overlay of the emission spectra of BC-DPP-1 upon excitation at 550 nm (slit 5 nm, Em. 560-900 nm, slit 5 nm) and 720 nm (slit 5 nm, Em. 730-900 nm, slit 5 nm), recorded in CHCl₃ at 25 °C

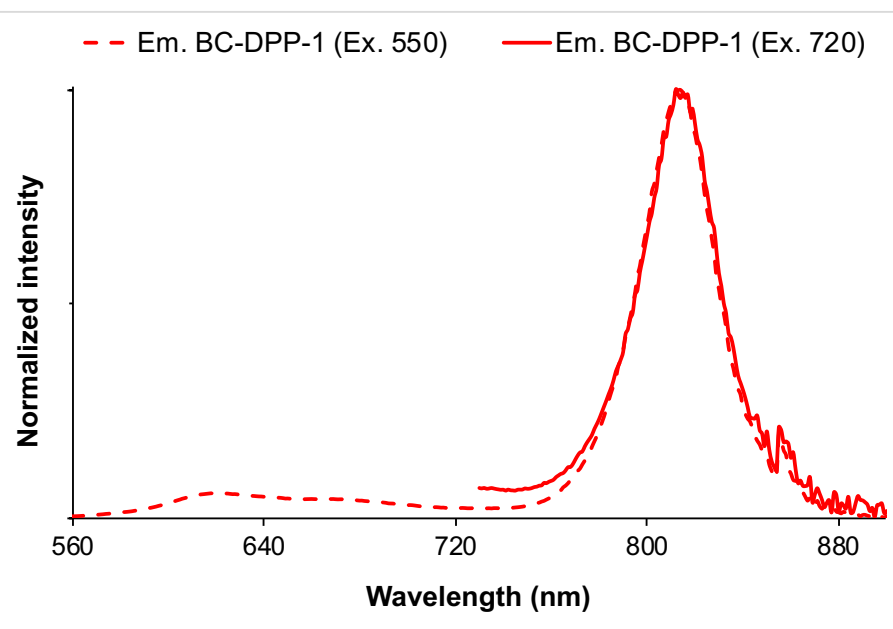


Fig. S41. Overlay of the absorbance spectra of diBr-BC, DPP 1 and BC-DPP-1 recorded in toluene at 25 °C

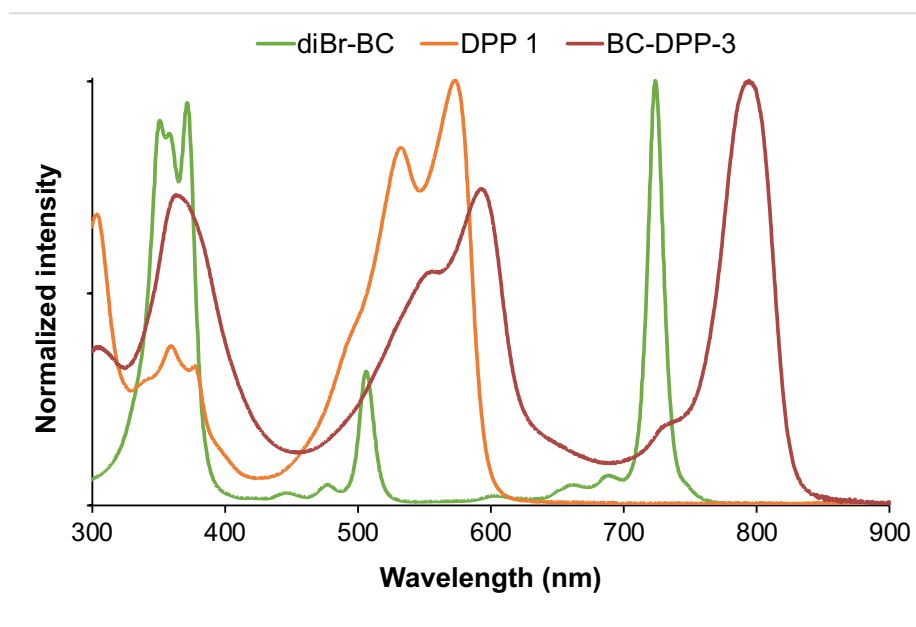


Fig. S42. Overlay of the emission spectra of BC-DPP-1 upon excitation at 550 nm (slit 5 nm, Em. 560-900 nm, slit 5 nm) and 720 nm (slit 5 nm, Em. 730-900 nm, slit 5 nm), recorded in toluene at 25 °C

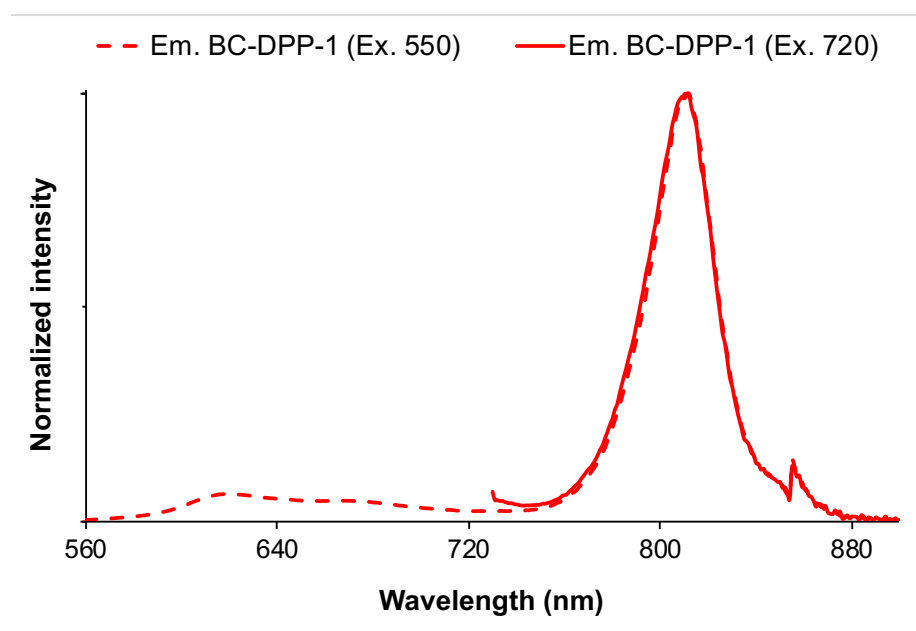


Fig. S43. Overlay of the absorbance spectra of diBr-BC, DPP 5 and BC-DPP-2 recorded in toluene at 25 °C

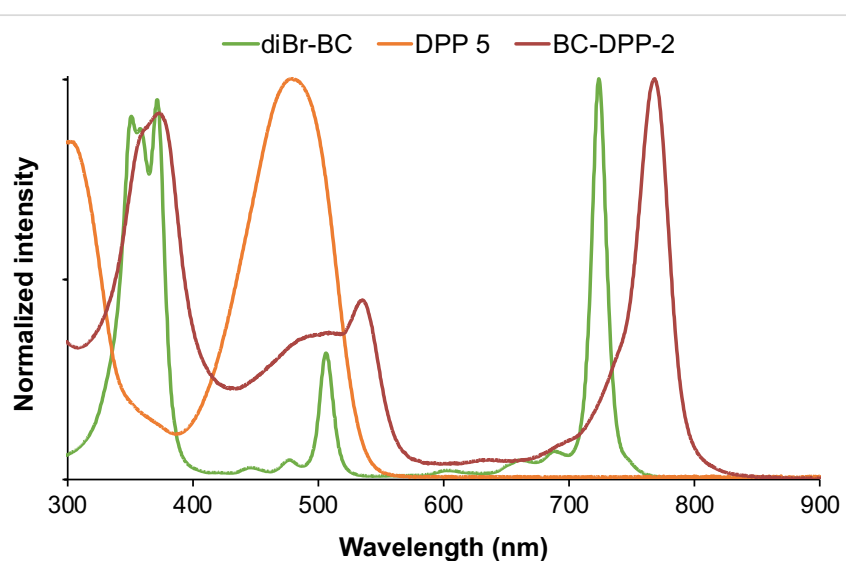


Fig. S44. Overlay of the emission spectra of BC-DPP-2 upon excitation at 450 nm (slit 5 nm, Em. 470-900 nm, slit 5 nm) and 690 nm (slit 5 nm, Em. 700-900 nm, slit 5 nm), recorded in toluene at 25 °C

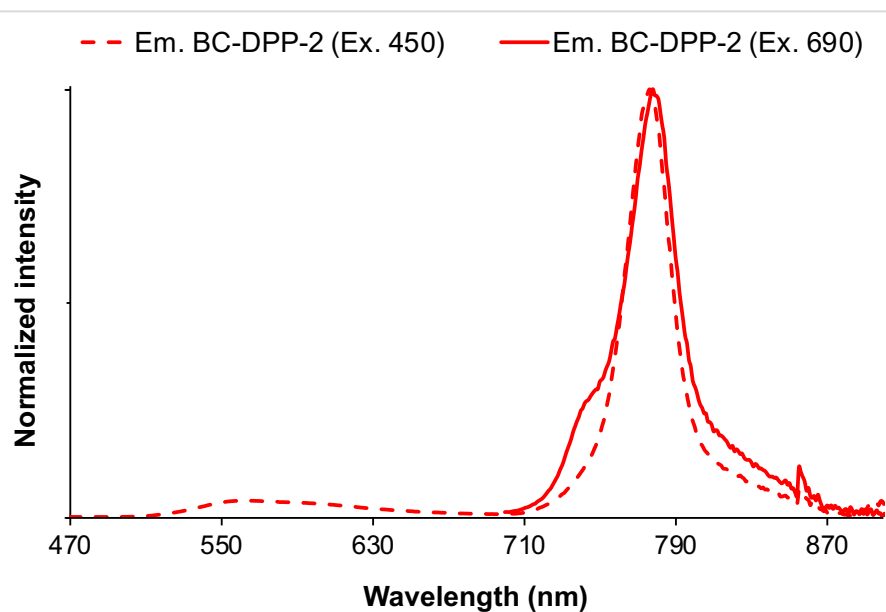


Fig. S45. Overlay of the absorbance spectra of diBr-BC, DPP 7 and BC-DPP-3 recorded in toluene at 25 °C

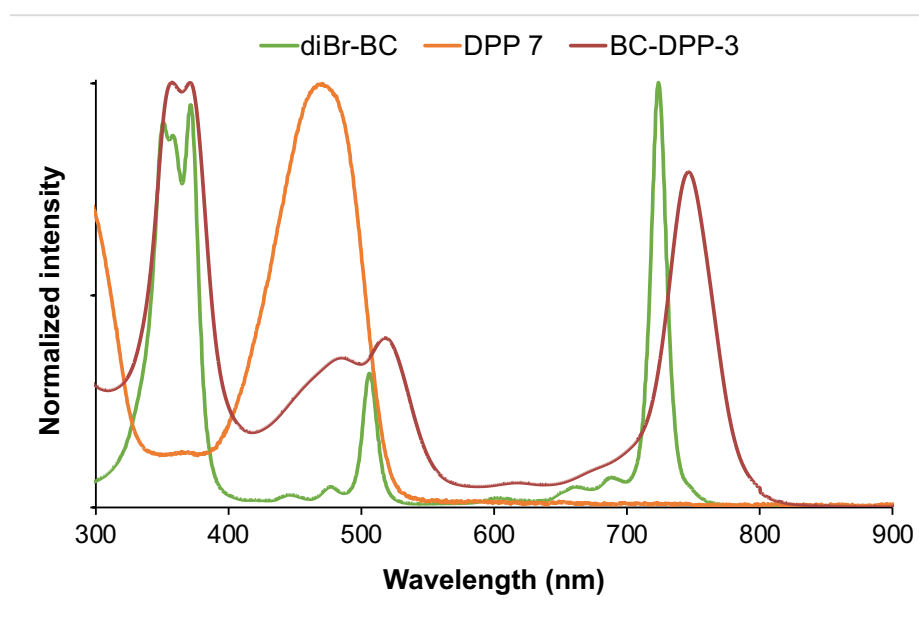


Fig. S46. Overlay of the emission spectra of BC-DPP-3 upon excitation at 450 nm (slit 5 nm, Em. 470-900 nm, slit 5 nm) and 680 nm (slit 5 nm, Em. 690-900 nm, slit 5 nm), recorded in toluene at 25 °C

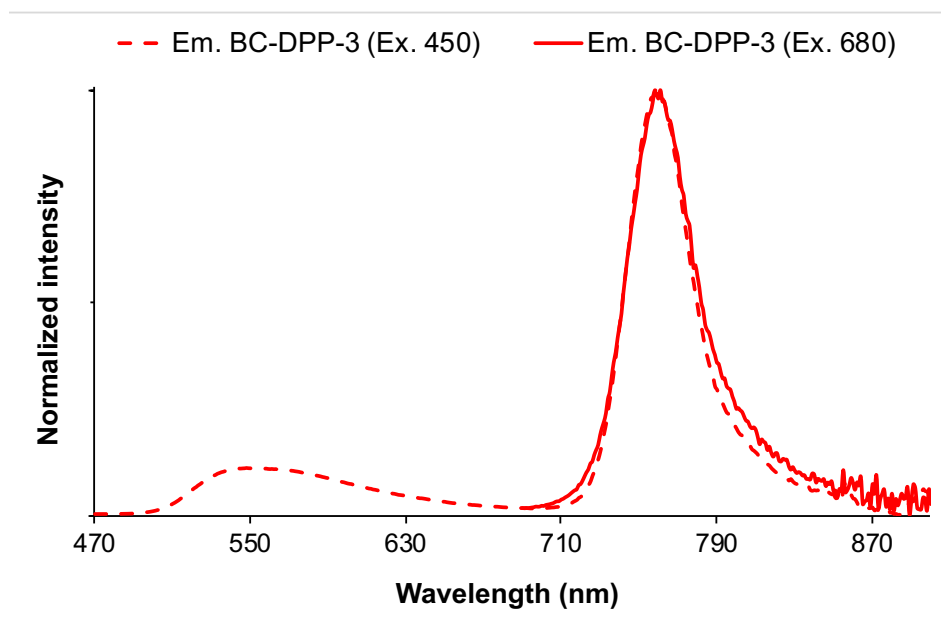


Fig. S47. Overlay of the absorbance and excitation (Em. 835 nm, slit 5 nm ; Ex. 300-825 nm, slit 12 nm) spectra of BC-DPP-1 recorded in CHCl₃ at 25 °C

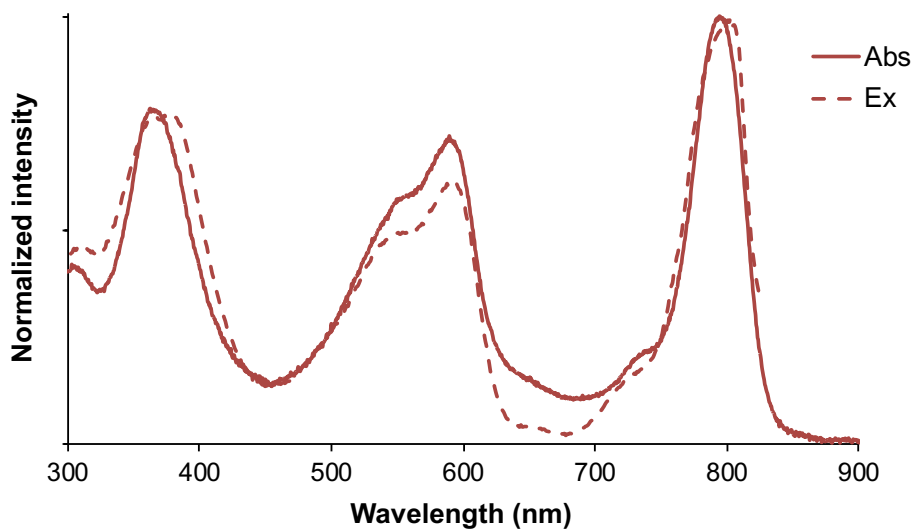


Fig. S48. Overlay of the absorbance and excitation (Em. 835 nm, slit 5 nm ; Ex. 300-825 nm, slit 12 nm) spectra of BC-DPP-1 recorded in toluene at 25 °C

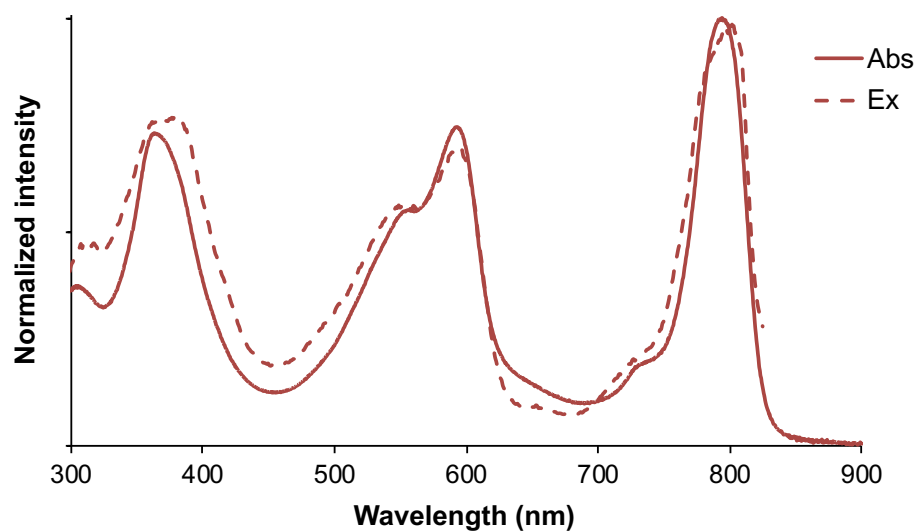


Fig. S49. Overlay of the absorbance and excitation (Em. 835 nm, slit 5 nm ; Ex. 300-825 nm, slit 12 nm) spectra of BC-DPP-2 recorded in CHCl₃ at 25 °C

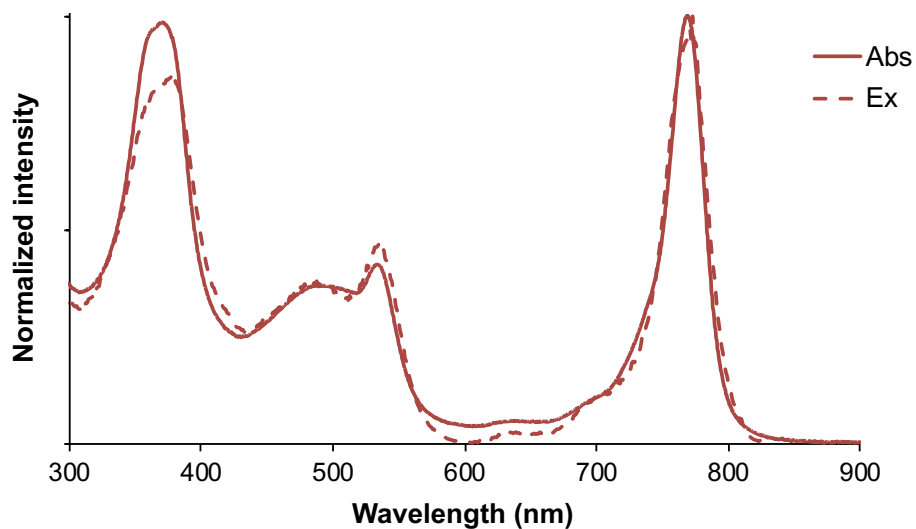


Fig. S50. Overlay of the absorbance and excitation (Em. 835 nm, slit 5 nm ; Ex. 300-825 nm, slit 12 nm) spectra of BC-DPP-2 recorded in toluene at 25 °C

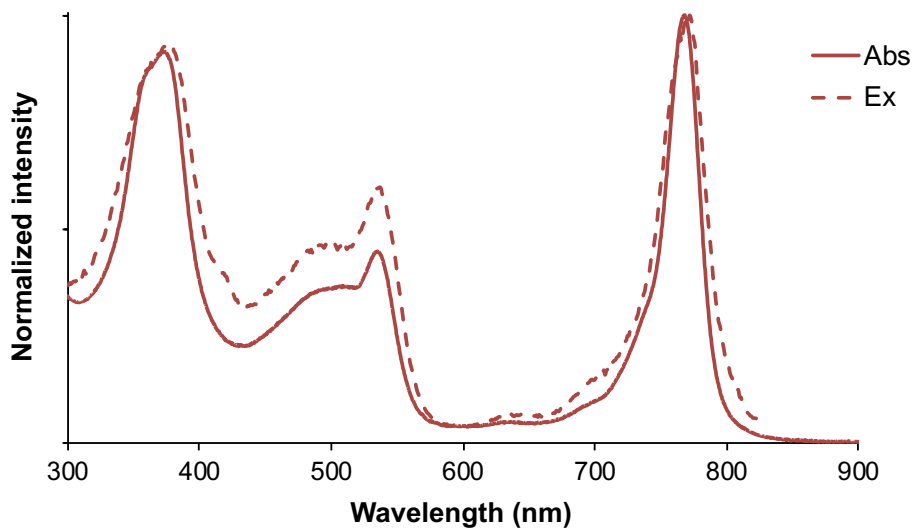


Fig. S51. Overlay of the absorbance and excitation (Em. 835 nm, slit 5 nm ; Ex. 300-825 nm, slit 12 nm) spectra of BC-DPP-3 recorded in CHCl₃ at 25 °C

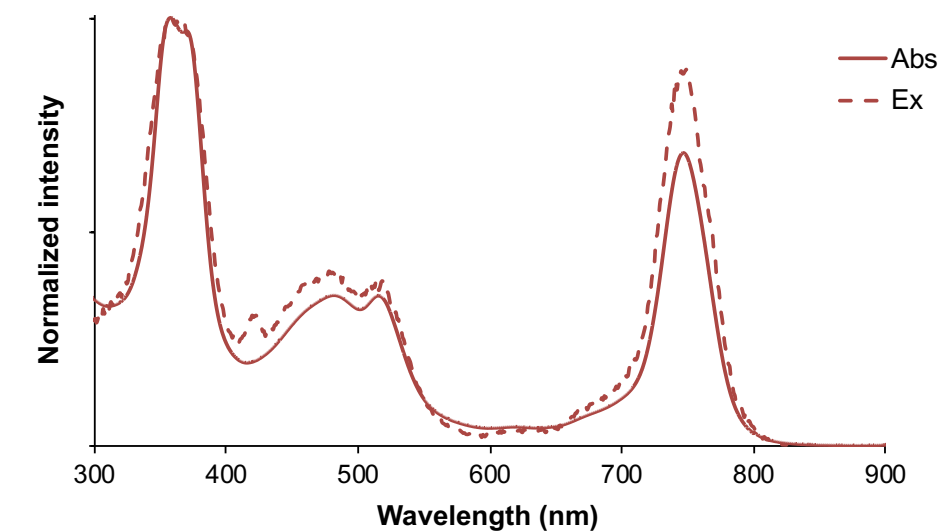


Fig. S52. Overlay of the absorbance and excitation (Em. 835 nm, slit 5 nm ; Ex. 300-825 nm, slit 12 nm) spectra of BC-DPP-3 recorded in toluene at 25 °C

